ARTICLE

A CFD Study of the Resistance Behavior of a Planing Hull in Restricted Waterways

Ahmed O. Elaghbash[*]

RSC for engineering and naval architecture and consultancy, Sudan

ARTICLE INFO	ABSTRACT
	The demand for high-speed boats that operating near to shoreline is increasing nowadays. Understanding the behavior and attitude of high-speed boats when moving in different waterways is very important for boat designer. This research uses a CFD (Computational Fluid Dynamics) analysis to investigate the shallow water effects on prismatic planing hull. The turbulence flow around the hull was described by Reynolds Navier Stokes equations RANSE using the k-ε turbulence model. The free surface was modelled by the volume of fluid (VOF) method. The analysis is steady for all the ranges of speeds except those close to the critical speed range Fh =0.84 to 1.27 due to the propagation of the planing hull solitary waves at this range. In this study, the planing hull lift force, total resistance, and wave pattern for the range of subcritical speeds, critical speeds, and supercritical speeds have been calculated using CFD. The numerical results have been compared with experimental results. The dynamic pressure distribution on the planing hull and its wave pattern at critical speed in shallow water were compared with those in deep water. The numerical results give a good agreement with the experimental results whereas total average error equals 7% for numerical lift force, and 8% for numerical total resistance. The worst effect on the planing hull in shallow channels occurs at the critical speed range, where solitary wave formulates.

1. Introduction

In this chapter, try to interpret the operation theory of high speed craft which considers the planing hull as the main part of it. Also, it is displayed an objective, purposes of the research, and thesis structure.

1.1 High-speed Craft

Many researchers have tried to define high-speed vessels; the first one is Baird (1998) who says the speed of

the ship up to 30 knots. Also, some hydrodynamicists say when the Froude number $Fn = U/\sqrt{g*L}$ above 0.4 such as high-speed monohulls and catamarans. Recently, definition of high speed craft, it means a craft that is operable on or above the water and has characteristics so different from those of conventional displacement ships, to which the existing international conventions, particularly SOLAS, apply, that alternative measures should be used to achieve an equivalent level of safety. In order to be considered a high speed craft, the craft must be

---

Corresponding Author:

Ahmed O. Elaghbash,

RSC for engineering and naval architecture and consultancy, Sudan

Email: men.aom90@gmail.com

capable of a maximum speed equal to or exceeding V = 3.7 displ .1667, where V is the maximum speed and displ is the vessel displacement corresponding to the design waterline in cubic meters. The classification of high-speed vessels depends on the forces carrying them; Figure 1 shows these forces which support the vessels. On the left-hand side, show the vessels supported by air, which includes Air Cushion Vehicles (ACV), Surface-Effect Ships (SES) and wing-in-ground craft (WIG).
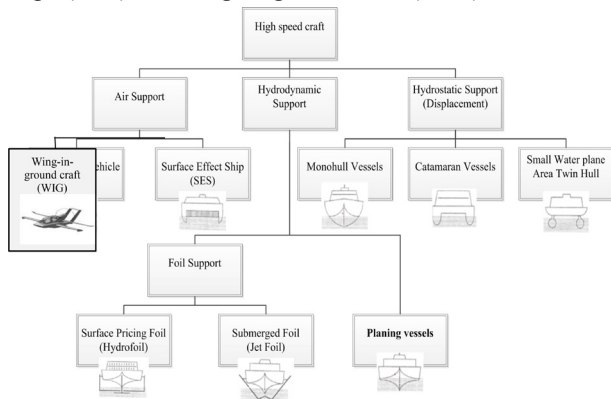
Figure 1. types of high speed craft

On the right-hand side, the Vessels are supported by a hydrostatic force which is given from the submerged part of the vessel (buoyancy), called Displacement vessels include conventional monohull, catamaran, trimaran, small water-plane-area twin-hull (SWATH). In between displacement vessels and air-supported, there is a hydrodynamics force supported vessels as a result of vessel forms such as planing hull or foil support including the surface pricing foil (Hydrofoil) and Submerged Foil (jet foil). They all suffer from the common problem of limited payload and sensitivity to wind and sea state. While each type of vessel has its unique characteristics depended to form of the vessel.

1.1.1 Wing-in-ground (WIG) Craft

Wing-in-ground (WIG) crafts are supported in their main operational mode solely by aerodynamic forces which enable them to operate at low altitude above the sea surface but out of direct contact with that surface. Accordingly, their arrangement, engineering characteristics, design, construction and operation have a high degree of commonality with those characteristics of aircraft. However, they operate with other waterborne craft and must necessarily utilize the same collision avoidance rules as conventional shipping. WIG craft is a multimodal craft which, in its main operational mode, flies by using ground effect above the water or some other surface, without constant contact with such a surface

and supported in the air, mainly, by an aerodynamic lift generated on a wing (wings), hull, or their parts, which are intended to utilize the ground effect action [1]. WIG crafts are categorized according to the following types:

• Type A: a craft which is certified for operation only in ground effect. Within prescribed operational limitations, the structure and/or the equipment of such a craft should exclude any technical possibility to exceed the flight altitude over the maximum vertical extent of ground effect.

• Type B: a craft which is certified for main operation in ground effect and to temporarily increase its altitude outside ground effect to a limited height, but not exceeding 150 m above the surface, in case of emergency and for overcoming obstacles.

• Type C: a craft which is certified for the same operation as type B; and also for limited operation at altitude exceeding 150 m above the surface, in case of emergency and for overcoming obstacles.

IMO and the International Civil Aviation Organization (ICAO) have agreed that any WIG craft capable of sustained flight outside the influence of ground effect should also be subject to the rules and regulations of ICAO. Other crafts, including those with limited "fly-over" capability, should be covered only by the maritime regulatory regime.

1.1.2 An Air Cushion Vehicle (ACV)

An Air Cushion Vehicle is a vessel that is completely carried by air pressure, in the near vicinity to the surface. It is suitable for utility over earth or water. Its flexibility makes it a vehicle of choice in circumstances where region remoteness, insufficient water profundity, or need of shoreline facility. To hold the cushion of air under the boat, it is outfitted with an elastic seal called a skirt. Air leakage out from down the skirt compensated by lift fans. The air pressure under the boat should be a balance for load weight on the boat.

1.1.3 Surface Effect Ships (SES)

A Surface Effect Ship operates merely above water and a little portion displacement, about 10%, is propped by catamaran-similar side hulls. This sort of vessel features a shallow draft than a routine catamaran and due to the minimal displacement, makes significantly less wake. Cause to the fixed side hulls, a SES has elastic seals only at the stern and bow and demand lower lift capacity than an ACV.

1.1.4 Jet Foils and Hydrofoils

Jet foils and hydrofoils have a more profound displac-

ement than SES, ACV, and trend to be steadier, giving a smoother traveler ride. Hydrofoils fly on wings in the water: whereas, hovercraft float on a layer of air above the water. Cause of their deeper displacement they are also more susceptible to damage from floating debris. Foils extend from movable arms that act as the lifting surface at operational speeds. The foils make a lift that completely raises the monohull out of the water. Hydrofoil parts can be partitioned into two main classifications, surface-piercing and completely submerged. A hydrofoil must be able to function securely while both hulls are borne mode and while takeoff.

1.1.5 Planing Hull Vessels

The vessel lifted by bouncy at Froude number under 0.4 is called a displacement ship. Whereas when carrying most of the weight of the ship by hydrodynamic force at Froude number above to 1 it's called a planing vessel. While the semi-planing vessel is in the range of Froude number between 0.4 and 1. Planing craft is employed as navy boats, racing boats, service boats, recreational boats, and ambulance boats. In general, the planing hull sailing with trim by stern means rise the bow and immerse the stern as a result of planing surface. Figure 2 shows the hydrodynamic force push the planing hull outer the water to reduce the resistance and increase the speed.
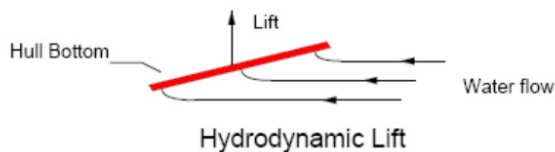
Figure 2. hydrodynamic lift of planing hull

1.1.6 Monohull Vessels

Adjusted from the army, the high execution monohull design can be seen in corvettes and destroyers. These vessels are distinguished by a slim limit hull, high speed, and the capacity to function in shifted climate conditions. Whereas exceedingly maneuverable, this sort of vessel is delicate to wind and wave activity unless stabilizers are utilized. The fast ship design is an illustration of a high execution monohull design, and Norasia is a case of a monohull with stabilizers. This design offers the highest cargo carrying capacity per ton. Most monohulls vessels work on comparatively lower ranges of speeds.

1.1.7 Catamaran Vessels

A catamaran vessel has two displacement hulls. It utilizes when required for a spacious area on the deck and high stability in sailing. This feature is comfortable for a passenger, and suitable for low-density cargoes. For that, it uses in fast ferries.

• Asymmetrical Catamarans: The more prevalent basic form of a multihull in the 1970s than nowadays. It is a monohull vessel with a slot cut out within the center.

• Symmetrical Catamarans: An amended catamaran design with many hull shape variations that feature two symmetrical hulls. This improves the performance and course keeping of the asymmetrical catamaran. This multihull is designed to move a range of displacement speeds semi-displacement speeds. Always, the level of the main deck is higher than operational waterline leading to improve sailing at rough sea, in comparison with Asymmetrical multihulls.

• Wave-Piercing Catamarans: this design populates by INCAT of Australia. It is asymmetrical multihulls with an elongated bow-section. The bow-section designs have many versions, notices hard taper at the end. It is designed to work under the waterline and the after sections operate in a displacement/semi-displacement mode. Since water is more stable on the underwater surface, the wave-piercing catamaran has excellent exposed water performance.

1.1.8 Small Water-plane Area Twin Hull (SWATH)

Small water-plane Area Twin Hull is considered an amendment of a catamaran design. Its design is recognized by two tubular immersed in water under hulls, fixed to the upper catamaran frame by slim struts. The torpedo-shaped hulls work beneath the waterline. The concept is to put the ship's buoyancy under the water surface and give minimal surface region at the waterline for waves to act upon, creating great sea-keeping capacity.

1.2 Objectives of Research

This work is shedding light on The CFD capability measurements to capture all phasic and phenomena in different waterways. Furthermore, the shallow channel hydrodynamic forces effect on planing prismatic hull compared with hydrodynamic forces in open water; this was conducted through a transition from displacement speed to planing speed.

1.3 Purposes of Research

The following questions are addressed in this thesis.

• How accurately can the hydrodynamic forces on a planing hull be predicted using CFD simulations?

• Do the CFD simulations yield any additional information that is not obtained from model testing?

• What are phenomena which occur in the free surface during moving the planing hull in different waterways for

a transition from displacement to planing speed?

1.4 Thesis Structure

The thesis is divided into six chapters:

Chapter 1 includes the dividing of high-speed vessels depending on type of force which supported vessel, three main forces; Air support, hydrodynamic support, and buoyancy support. Also, it is displayed an objective and purposes of research, and thesis organization.

Chapter 2 includes the literature reviews of planning hull analysis techniques used to obtain hydrodynamic performance in various waterways. Besides, the Savitsky formula is applied to a prismatic planing hull is presented.

Chapter 3 Introduce the theory of planning hull, it explained the main characteristics and the form types of a planing hull. Also, it shows resistance types on a planing hull, and effect of confined water to wave pattern and viscous resistance.

Chapter 4 covered the steps of CFD analysis; domain dimension selection, boundary condition siting, and grid generation strategy which is used finite volume method for prismatic planing hull analysis, when sailing through the shallow channel and open water.

Chapter 5 discusses and validates numerical results obtained from a shallow water channel include wetted length, total resistance, hydrodynamic lift force, normal force, and wave pattern with experimental results. Also; compares total resistance and wave form with open water results.

Chapter 6 includes conclusion for sailing effect in various waterways of planning vessel and recommendations for future works.

2. Literature Review

This chapter reviews the techniques which using for planing hull analysis. Besides, the Savitsky formula is applied to a prismatic planing hull is presented.

2.1 Background

Recently, the simulation of the hydrodynamic performance of planing hull sailing in shallow water has become a common practice in the yachts building community. Hence, it is more used for the high-speed boats which sailing near to shoreline compared with where yachts used to navigate before. The high demand for high-speed boats operating near shore requires good knowledge of their behavior in three regions of speed, (subcritical, critical, and supercritical).

There are many methods to calculate hydrodynamic characteristics of planing vessels such as analytical experimental
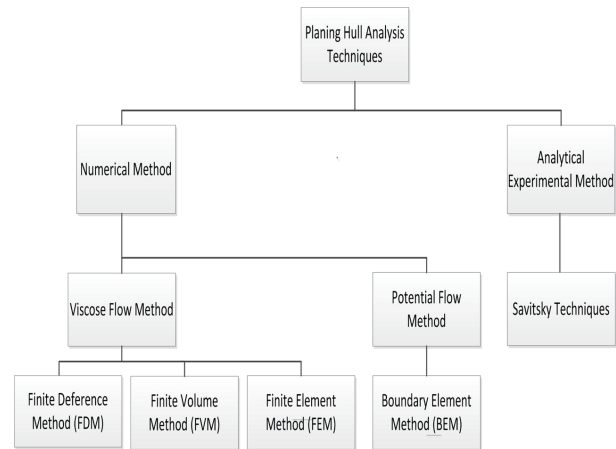
Figure 3. analysis approaches used for planning hull [2]

and numerical methods Figure 3 shows the most common of these methods including the numerical and experimental methods. The experimental methods require expensive facilities and measurement tools. These results increased cost and time compared with the numerical methods. Hence there has been an increase in the use of numerical methods for investigating the small boat resistance in different waterways such as shallow channels and open water. At the planing speed, the planing hull is supported by buoyancy force and lift force which put the hull in position, the wave-making resistance is the main component in the total resistance. The waves system includes the transverse wave and the divergent wave. The divergent wave angle starts for a 19.47 degree at subcritical speed (Kelvin wave pattern) and increases until 90 degrees at critical speeds after that decreases in supercritical speeds.

The first theoretical formula to consider the calculation of maximum pressure around planing 2D sections was proposed by Kerman [3], which was based on the conservation of momentum in the analysis. His work remained in use until equations for 3D planing surfaces by Savander and Scorpio [4] were introduced, which describes potential perturbation and vortex distribution around a planing plate.

The finite difference method was used to solve the Kadomtsev-Petviashvili equation for a TSS model moving near critical speed [5]. By using the technique of matched asymptotic expansions along with nonlinear shallow-water wave theory, the problem is reduced to a Kadomtsev-Petviashvili equation in the far-field, matched with a near-field solution obtained by an improved slender-body theory, taking the local wave elevation and longitudinal disturbance velocity into account. The ship can be either fixed or free to squat. Besides wave pattern and wave resistance, the hydrodynamic lift force and

trim moment are calculated by pressure integration in the fixed-hull case; running sinkage and trim, by the condition of hydrodynamic equilibrium in the free-hull case. Many experiments were conducted in an attempt to calculate the force and the moment on the flat bottom hull in shallow water at fixed trim by Christopher [6]. Furthermore, the force and moment on a constant deadrise angle prismatic hull by Reyling [7] were obtained experimentally.

For series 62 hull form, residuary resistance was computed over a range of speeds from displacement speeds to planing speeds when the hull moving in shallow water and it was concluded that there is an increase in residual resistance at the subcritical speed range and a decrease at the supercritical speed range as compared to deep water. Besides, there was a resistance hump created at the maximum angle of trim and the highest value of sinkage.

The 2D+t potential flow method was used to investigate the performance of planing hulls in calm water and was compared with 3D Reynolds Navier Stokes Equation (RANSE) method by Iafrati and Broglia [8]. A comparison between the two solutions is established to understand the role played by three-dimensional effects, neglected within the slender body assumption. The analysis is focused on the evaluation of the free surface shape and of the pressure field acting on the hull surface. It is shown that a good agreement is achieved in terms of the free surface profile, corrected is applied to the 2D+t solution to account for the rise up of the water in front of the hull. The comparison in terms of pressure distribution reveals important three-dimensional effects in the very fore part of the hull, in the region about the separation point, and at the transom. These methods-based designs were presented, starting from a non-stepped hull configuration, a multiple-step solution was developed and an optimization of the unwetted aft body area behind the steps was performed. The goal of the optimization is drag reduction and dynamic stability [9]. The validation of the 2D+t model for single stepped planing hull with the experimental data in terms of; resistance, dynamic trim, and wetted surface area was carried out by Bilandi [10]. The obtained hydrodynamic results have been compared against the experimental data and it has been observed that the presented mathematical model has reasonable accuracy, in particular, up to Froude number 2.0. Furthermore, this mathematical model can be a useful and fast tool for the stepped hull designers in the early design stage to compare the different hull configurations. It should also be noted that the mathematical model has been developed in such a way that it has the potential to model the sweep-back step and transverse the vertical motions of single-stepped planing hulls in future studies.

The RANSE method was used to predict moment and force on a planing prismatic hull with a constant deadrise angle equal to 20 degrees by Brizzolara and Serra [11]. Results obtained, in terms of drag lift forces and longitudinal trimming moment, are compared with available experimental (model tests made at Hydronautics towing tank) and semi-empirical theories (Savitsky, Shuford, etc.) commonly used by a naval architect for the prediction of planing surface hydrodynamic performance. By the comparison of global force components and moments and the analysis of distributed parameters, such as pressure on the wetted hull, tangential stresses, spray root line, and wave elevations, some interesting conclusions can be drawn on the accuracy of CFD codes for the prediction of steady hydrodynamic performance of planing hulls.

Safari calculated; total resistance, added resistance, and wave pattern numerically for model 4667-1 by using CFD software based on finite volume method to solve the RANS equations in different speed and depths including deep and shallow water conditions. Also, the wave pattern and flow field around the vessel are investigated. For validating the method, at first, the resistance results in deep water are compared with the experimental data and show good agreements. Simulations are performed in transient mode, using Volume of Fluid (VOF) and k -ε schemes to model the free surface turbulent flow. The results have shown that by decreasing the depth, the shallow water-resistance of a planing vessel will be increased [12]. Mancini used this analysis to get; total resistance coefficients, wetted surfaces, and dynamic trim for the parent hull model (C1 hull) from the Naples Systematic Series (NSS), Form hull characterized by a warped bottom [13].

Moreover, heave motion, pitch angle, free surface deformation, and resistance of planing vessels were obtained through this analysis by Wang [14] in deep water.

The modern transverse stepped planing hull was investigated by CFD, which applies moving mesh techniques and large eddy simulation to find the total resistance, trim, and sinkage. These numerical results were validated with experimental results [15]. Moreover, Bakhtiari estimated; the numerical results of drag, pressure distribution, wetted surface, water spray, and wave generation by stepped planing hull [16]. Furthermore, the wake profile was compared by Savitsky and Morabito empirical formula. The morphing mesh method and k-ε model were used to simulate the fluid flow around the two-stepped hull moving freely to heave and pitch [17]. Also, this mesh technique was used to describe hydrodynamic characteristics around the tunneled planing hull and it's

compared with experimental results [18].

The Smoothed Particle Hydrodynamics (SPH) method investigated the pressure distribution on the seafloor in very shallow water and, the change in the angle of created divergent waves over a range of speeds [19].

2.2 Savitsky's Method

This analysis for prismatic planing hull at fixed trim and fixed beam aims to find formulas for calculating the lift force, total resistance, wetted area, and center of pressure. There are two steps for this analysis, a simple case that imposes that all forces and moment affect in the center of gravity. Next, the general case includes lift, drag, and trust effect in a different point on the hull.

The equations are depended on huge experimental results. The lift coefficients equation following as [20]

$$C_{L\beta} = C_{L0} - 0.0065\beta C_{L0}^{0.6} \qquad (2.1)$$

And

$$C_{L\beta} = \frac{F_{L\beta}}{0.5\rho U^2 B^2}$$

Also

$$C_{L0} = \frac{F_{L0}}{0.5\rho U^2 B^2} = \tau_{deg}^{1.1}\left(0.01\lambda_w^{0.5} + \frac{0.0055\lambda_w^{2.5}}{C_v^2}\right) \qquad (2.2)$$
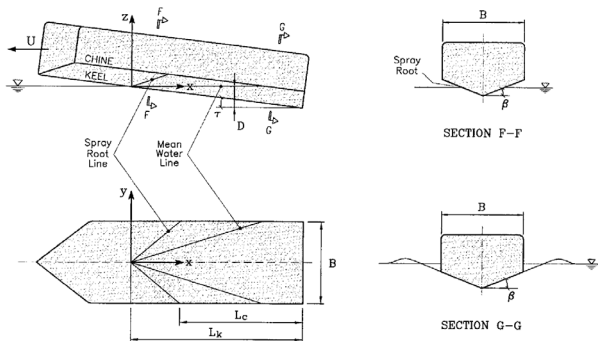
Figure 4. parameters for prismatic planing hull by Savitsky (1964)

Figure 4 interpreted the dimensions and trim angle τ and deadrise angle β which are used to define the Savitsky geometry. From Savitsky formula notices that the lift force and drag is quale zero when the planing hull even keel. The drag force can be found by

$$Rp = F_{L\beta}\tau \qquad (2.3)$$

The angle of trim has an important role to make the hull similar to a hydrofoil. It means that the hull has a drag force and lift. Moreover, the deadrise angle βis decreased lead to an increased lift force part. Finally, the longitudinal center of pressure calculates by

$$\frac{l_P}{\lambda_w B} = 0.75 - \frac{1}{5.21 C_v^2/\lambda_W + 2.39} \qquad (2.4)$$

Where lp the distance from the stern to the center of pressure

The total wetted bottom area of a planning surface is

actually divided into two regions. One is aft of the spray-root line, commonly referred to as the pressure area and the other is forward of the spray-root line, referred to as spray area. The pressure area is load carrying area of the planning bottom. The forward spray area contributes to the total drag but is not considered to support any portion of load. An enlarged sketch of flow direction on a deadrise surface is shown in Figure 5. It is found that the flow in the pressure area is predominantly aft with some transverse floe along the chines. The flow along the spray-root line is primarily along the direction of the stagnation line. In the spray wetted area the direction of the fluid flow are such that the space angle between oncoming fluid particles and stagnation line is equal to the angel between the direction of the spray jet and the stagnation line; for example any line of motion in the spray area is nearly a reflection about the stagnation line of the incidence velocity direction. Since the pressure in the spray area is nearly atmospheric, then, by Bernoulli, the spray velocity can be assumed to be equal to the planing speed.
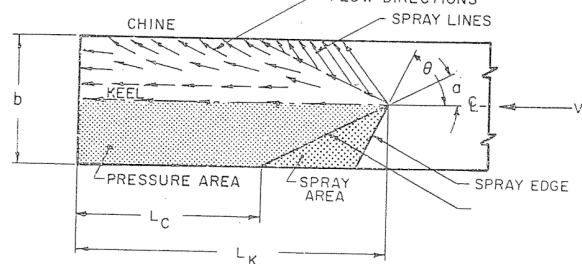
Figure 5. flow direction along planning prism and extent of spray area [20]

The total spray area, both sides, projected on a plane along the keel line is given by

$$A_s = \frac{b^2}{2}\left(\frac{tan\beta}{\pi tan\tau} - \frac{1}{4\,tan\Phi\,cos\beta}\right) \qquad (2.5)$$

The Savistly formula achieved good agreement with the experimental results but the CFD method work at a different type of modern hull shape and various waterways.

3. Planing Hull Theory

This chapter displays the main characteristic of the planing hull and the type's form of planing vessel. It is defined the concept and types of resistances. Also, it shows the effect of restricted waterways on wave-making resistance and viscous resistance.

3.1 Planning Hull Characteristic

The planing vessels sharing with Common features have a transom stern, bow carve, flat surfaces, hard chines, V shape at the transom, and maximum length does not exceed 30m. Figure 6 shows the main characteristics of

the planing hull shape.
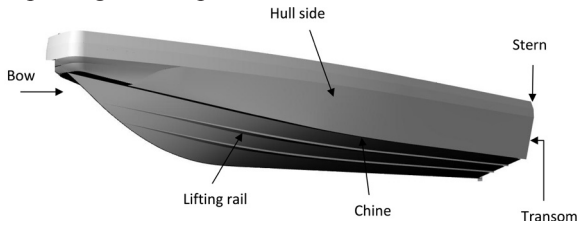
Figure 6. main planing hull characteristics

All the planing boat has one or more chine. It means the points crossing the bottom and hull-side. There are three types of chine; hard chine-like-angel, soft chine-like-carve, and reverse chine. A hard chine is meant to throw spray to the facets of the hull and to prevent water from flooding the hull where it will raise resistance. Chine with step has a considerable contribution of dynamic lift force. The soft chine gives smoother sailing for the hull compare with a hard chine boat. Whereas it is the maximum speed for hard chine boats higher than the soft chine boats [21].

Deadrise β is the angle a hull bottom makes with the horizontal plane viewed from ahead or astern. The right amount of deadrises gives a boat directional stability, a softer ride, and reduces wetted surface drag as the boat rises on a plane. Deadrise is said to be "constant" if it stays approximately the same from amidships to the transom. Deadrise is "variable" if it changes from a deep angle at amidships to a shallow angle at the transom.
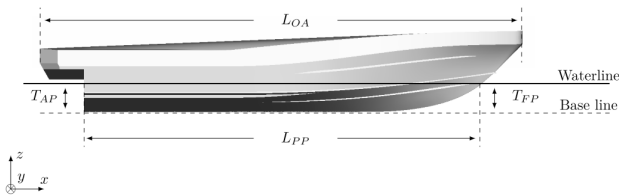
Figure 7. main dimension of planning hull

The dimensions of the planing hull are considered the part of hull characteristics shown in Figure 7.

L_{OA} Overall length of the planing hull measure the distance from bow to stern

L_{PP} Length between perpendiculars, it changes when the hull starts moving

T_{FP} Draft forward measure the vertical distance between the base line and waterline in a bow

T_{AP} Draft aft measure the vertical distance between base line and waterline in a stern

The hull upright position, means don't movies is

$$T_{AP} = T_{FP}$$

Trimming angel θ when the planning hull start go forward the bow rising and stern immersed.

$$T_{AP} \neq T_{FP}$$

3.2 Planing Hull Type

The design of the planing hull boat improves with time to provide comfort, luxury, and increase the speed according to customer requirements and application of vessels. There are a lot of designs of planing to improve the performance of the hull.

3.2.1 Prismatic Planing Hull

The Fridsma hull was produced in 1969 by the Davidson Laboratory. Figure 8 shows the form of a prismatic hull in which the deadrise angle β is fixed in all the stations and was one beam in length. The bow had identical planforms and elliptical keel profiles. When the β equals zero the hull is called the flat bottom.
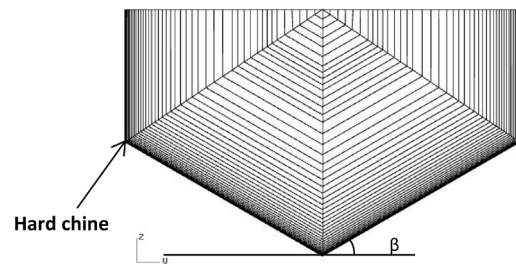
Figure 8. Prismatic Fridsma hull [22]

3.2.2 Warped Planing Hull

Figure 9 shows the warped hull in which the deadrise angle changes along the length of the hull, for that demand the change of angle along with any station. This gradual change of angles from bow to stern transom gets better comfortable on board and decreases fuel consumption on a warped hull compared with a prismatic hull in the voyage.
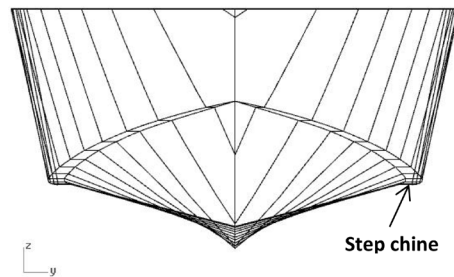
Figure 9. Warped hull of C945 models [23]

Through time the planing hull design developed to decrease the total resistance and increase the speed. For that on the warped bottom hull, a spray rail was added to improve which improves the performance of the planing hull by Müller-Graf (1991).

- Give more lift force due to the deflection of the spray.

- Decreases the spray frictional resistance to reduce the spray wetted area on the hull.
- Damping roll motion and more transverse stability.
- Increases deck dryness.

3.2.3 Tunneled Planing Hull

The tunnels divided the planning hull into three parts: the main hull and two side hulls. It is called a trimaran planning hull. Figure 10 shows the body plane of the tunneled planning hull. The tunnel gives an additional aerodynamic lift of the hull and less power required for racing.
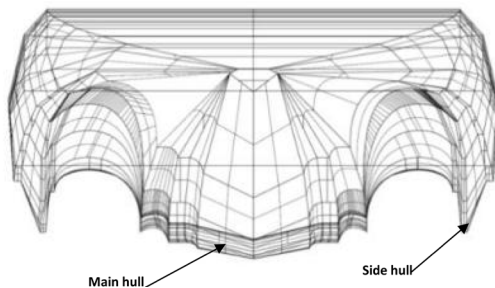
Figure 10. tunneled planing hull [18]

3.2.4 Stepped Planing Hull

The modern designs of the planing hull have one or more transverse steps on the hull bottom. The transverse step separates the flow of water and ventilates the aft part of the hull. This causes a reduction of the wetted surface area, which leads to decreased friction resistance and improves the lift per unit area. Furthermore, it gives damping pitch motion and improves pitch control. Figure 11 shows the planing hull with one transverse step. Approximately, the stepped planing gives good performance at the high-speed range $1.5 \leq Fn \leq 1.75$ and more drag at the displacement speeds compare with the same planing hull non-step.
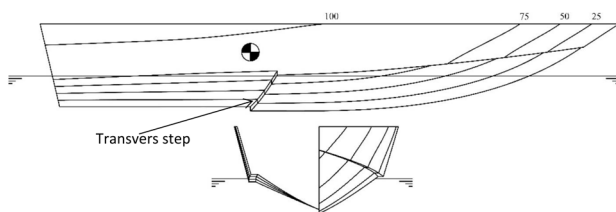
Figure 11. The C03 model buttock line and body plan [10]

3.2.5 Air Lubricated Planing Hull

This type of boat is a lot ordinarily referred to as a planing hull. When to move at high speed the bow lifts out of the water and is carried by the passage of air under that, whereas the stern is in a displacement mode and is carried by the seawater. It is sailing similar to small boats

and private watercraft.

3.3 Planing Hull Resistance

The total resistance for bare planing hull in calm water R_T excludes the added resistance by sea wave and wind. It is equal to the sum of the air resistance, viscous resistance, spray resistance, and wave-making resistance.

$$R_{T=}R_A+R_V+R_S+R_M \tag{3.1}$$

There is an effect of restricted waterways such as finite depth of water and baking effect. This waterway increases total resistance compared to the unrestricted waterway.

3.3.1 Air Resistance

The air resistance is very little value in which the density of air is much smaller than the density of water. Spatially at low speed can be neglected. The air resistance can be calculated by

$$R_A=0.5\rho_a c_D A U^2 \tag{3.2}$$

Where ρa the density of air, C_D air frictional coefficient, A projected area on vessel above the waterline which facing the air, U speed of a vessel.

3.3.2 Viscous Resistance

The viscous resistance R_V concerns the main component of total resistance because its value depends on tangential force on the hull and vessel form. The viscous resistance includes frictional resistance, R_F viscous pressure resistance R_{VP} and Flow separation. The frictional resistance can be calculated by

$$R_F=0.5\rho C_F S U^2 \tag{3.3}$$

C_F The frictional coefficient for smooth hull founded by the International Towing Tank Conference (ITTC) 1957 for model ship.

$$C_F = \frac{0.075}{(\log_{10} Rn-2)^2} \tag{3.4}$$

Reynolds number is equal whereas kinematic viscosity.

The factor (K) expresses all parameters related to the shape of the hull like the wake, the roughness of a surface, separation point, and eddies….etc.

$$R_V=(1+K)*R_F \tag{3.5}$$

To explain the impact of fluid viscosity, boundary layer theory can be used. This means that viscosity matters only in a thin layer close to the surface of the hull. It is possible to use the two-dimensional boundary layer along a flat plate to define significant viscous flow characteristics.

A flat plate can be approximate the moistened hull surface. If we look at the flow following the ship from a reference frame, the ship's ward speed appears as an incident flow on a stationary hull with velocity U, as shown in Figure 12.
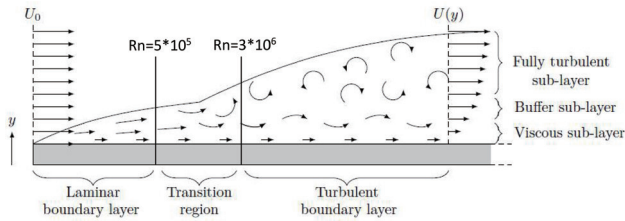
Figure 12. sachem of the boundary layer on a flat plate [24]

3.3.3 Spray Resistance

Almost, the spray resistance starts to occur at Froude number 0.5 and rapidly increases with speed. Its effect of the spray resistance was divided to pressure resistance component and frictional resistance by M¨uller-Graf (1991).

$$R_S = R_{SP}(Fn) + R_{SF}(R_n, W_n) \qquad (3.6)$$

Where R_{SP} The function of Froude number, R_{SF} the function of the Reynolds number and Weber number

$$Wn = \frac{\rho V_{SR}^2 d_{SR}}{T_S} \qquad (3.7)$$

V_{SR} is the spray velocity, d_{SR} is the spray thickness, and Ts is the surface tension at the water-air interface. A representative value of Ts

3.3.4 Wave Making Resistance

The wave-making resistance R_M is the second major component of the total resistance. It is the resistance of a wave, which is generated by the vessel when it moves in calm water. Three factors affect wave-making resistance: speed of the vessel, underwater hull form, and depth of water. The last factor that has a strong influence on Froude depth equal to one. The wave-making resistance cannot be easygoing for calculating it, like viscous resistance. Kelvin (1887) explain the waves system established when the pressure point moving in deep water. There are two types of waves. Figure 13 shows the divergent wave and the transverse wave in deep water. The crest divergent wave slopes 19.28º from the centerline. While the transverse wave perpendicular to the centerline 90º. However, it recently shows that this angle can be significantly smaller at large Froude numbers [25].
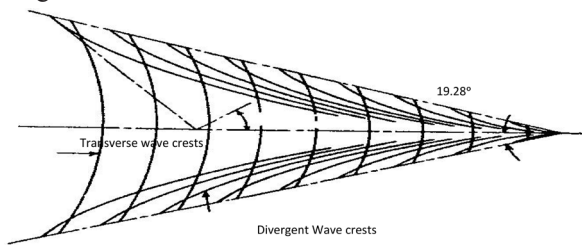
Figure 13. The Kelvin ship wave pattern in deep water. The included half-angle 19º28_ of the waves is called the Kelvin angle and is affected by the water depth [26]

3.4 Restricted Waterways Effect

The restricted waterways like the channels, lakes, harbored, and so on. Have effects on the total resistance, because there is a restriction on the depth of water and width or both. show the depth Froude number F_h makes the essential role in divide the range of speed into three regions in shallow water

$$F_h = U / \sqrt{g * h} \qquad (3.8)$$

• $F_h < 1$ the region of subcritical speed the wave pattern like in deep water.

• $F_h \approx 1$ the region of critical speed the divergent wave angle equals 90.

• $F_h > 1$ the region of supercritical the divergent wave angle equals 45 and disappear the transverse wave.

3.4.1 Effect on Wave-making Resistance

In shallow water, when increases the Froude depth F_h the wave angle modified means that change the angle of divergent wave and transverse in waves system shown in Figure 14. That is a modification in the wave system as a result of wave retardation which means the wave speed in shallow water decrease than the deep water. All of that leads to a change of wave-making resistance in shallow water. Especially, at critical speed in a shallow water channel can show the solitary waves. When Froude depth was equal to 1, the speed of the ship was equal to the speed of the wave, which can be calculated by

$$U = \sqrt{g * h} \qquad (3.9)$$
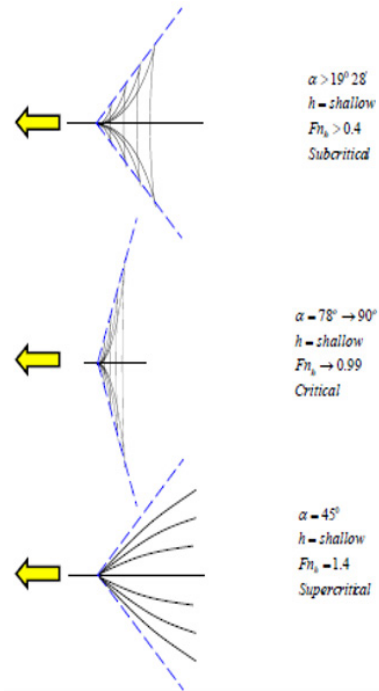
Figure 14. wave pattern change in shallow water

3.4.2 Effect in Viscous Resistance

In shallow water, according to throttling the flow between the seabed and bottom hull, The fluid flow under the vessel increased speed and decreases pressure supported the hull, it's called the backflow effect, the fluid speed rises leads to enhancement skin friction resistance, whereas decreases water pressure under the hull, its changes the position of the hull.

Squat phenomena definition is combined between sinkage and trim when the hull moving in shallow water, sinkage resulting from pressure dropping under the hull. It causes a change of water plane area and moves center of gravity. If the center of gravity union with from center of buoyancy, the hull is upright. When the center of gravity move from the center of buoyancy, a trim angle is established between them. For all that, squat effect to:

• Increases the total resistance, viscous resistance, and wave-making resistance when the vessel sailing forward.

• The ship sailing slow-speed and has been losing part of maneuvering and steering.

• There will be a drop in speed in shallow water as a result of increased resistance and reduced propulsion efficiency.

• There is a greater tendency towards vibration as a result of propeller-induced vibration.

A range of planing speed the hydrodynamic lift force work opposite direction to sinkage force. So the sinkage force reduces the buoyancy force which shares in put the planing hull in position.

4. Methodology of Analysis

In this chapter, the methodology used in the CFD analysis is described. The chart in Figure 15 shows the CFD results validation with experimental data. The work is started by defining the numerical domain dimensions. And then mesh elements are generated and boundary conditions for the numerical domain are set to carry out the analysis and obtain the results. Post-processing results are then assessed by comparing them to experimental data. If the results are in agreement with the experimental data the analysis is finished. Otherwise, modifications on mesh and setup are applied in the new analysis boundary condition and regenerating the mesh to make the new analysis until getting valid results.

4.1 Finite Volume Method

In this research work, the finite volume RANS code ANSYS CFX was used to study the flow around a small planing hull craft in a shallow water channel to predict the hydrodynamic forces and wave patterns of the hull at

subcritical, critical, and supercritical speeds.
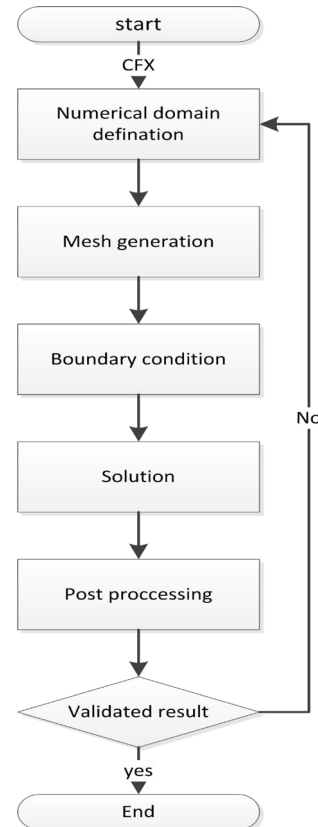
Figure 15. flow CFD analysis simulation

The motion of a viscous fluid is governed by the Navier-Stokes equations, which are valid both for turbulent and laminar flow. For an incompressible, Newtonian fluid in three dimensions under the influence of an external gravitational field, [27] the Navier-Stokes read.

$$\frac{\partial U_i}{\partial x_i} = 0.0$$

$$\frac{\partial U_i}{\partial t} + U_j \frac{\partial U_i}{\partial x_j} = -\frac{1}{\rho}\frac{\partial P}{\partial x_i} + \nu \frac{\partial^2 U_i}{\partial x_j \partial x_j} + g_i \qquad (4.1)$$

Here, the equations are formulated using tensor notation. The indices i and j in the Navier-Stokes equations run over the spatial coordinates x, y, and z. In these equations, U_i is the velocity in direction i, xi is the spatial coordinate in dimension i, t is time, ρ is the density, P is the pressure, ν is the kinematic viscosity and g_i is the gravitational acceleration.

The finite volume method (FVM), is a numerical method of discretizing a continuous partial differential equation (PDE), into a set of algebraic equations. The first step of discretization is to divide the computational domain into a finite number of volumes, forming what is called a mesh or a grid. Next, the PDE is integrated into each volume by using the divergence theorem, yielding an algebraic equation for each cell. In the centers of the cells, cell-averaged values of the flow variables are stored in so-called

nodes. This implies that the spatial resolution of the solution is limited by the cell size since the flow variables do not vary inside a cell [28]. The FVM is conservative, meaning that the flux leaving a cell through one of its boundaries is equal to the flux entering the adjacent cell through the same boundary. This property makes it advantageous for problems in fluid dynamics [29].

A stationary transport equation involving diffusion and convection of a general flow variable, variable, φ, can be written as

$$\rho U_i \frac{\partial \phi}{\partial x_i} = \frac{\partial}{\partial x_i}\left(\Gamma \frac{\partial \phi}{\partial x_i}\right) + S(\phi) \qquad (4.2)$$

Where Γ is the diffusivity and S is a source term that may depend on . By using the FVM, this equation can be written in discrete form as

$$a_P \phi_P = \sum_{nb} a_{nb} \phi_{nb} + S_U \qquad (4.3)$$

Where

$$a_P = \sum_{nb} a_{nb} - S_P \qquad (4.4)$$

In these equations, where the summations run over all the nearest neighbors of each cell, ϕ_P is the value of the flow variable in the present cell and ϕ_{nb} are the values of the flow variable in the neighboring cells. S_U and S_P are the constant and flow variables depending on parts of the source term, respectively. Furthermore, a_P is the discretization coefficient associated with the present cell, and are discretization coefficients describing the interaction with its neighboring cells. The discretization coefficients depend on the discretization schemes used to approximate the values of the flow variables on the cell boundaries, also known as cell faces. By using appropriate discretization schemes to determine the coefficients, a set of algebraic equations for the cell values is obtained.

4.2 Turbulence

When a hull is moving through the water, the flow around the hull is turbulent. In this section, the governing equations of turbulent flows are presented and turbulence modelling is explained.

4.2.1 Turbulent Flow

Turbulence has no physical definition, but it is characterized as a three-dimensional, irregular flow where turbulent kinetic energy is dissipated from the largest to the smallest turbulent scales. On the smallest turbulent scales, known as the Kolmogorov scales, the energy is dissipated into heat due to viscous forces. Since turbulence is a dissipative phenomenon, energy must be continuously supplied to maintain a turbulent flow.

Analytical solutions to the Navier-Stokes equations only exist for a limited number of simple cases such as laminar flow between flat plates. For turbulent flows in engineering applications, analytical solutions do not exist and the Navier-Stokes equations must be treated numerically. If they are solved using direct numerical simulation (DNS), the velocity field of the flow is obtained. However, since turbulence occurs on a wide range of time and length scales, DNS requires very high temporal and spatial resolutions to capture all the details of the flow. Thus, DNS is very computationally expensive and time-consuming which limits the method to special applications such as academic research or simulation of simple flows.

4.2.2 Turbulence Modelling

The most common way of treating turbulence is to use turbulence models in which the turbulent features of the flow are not resolved in time. By performing Reynolds decomposition, the instantaneous velocity and pressure can be decomposed as

$$u = U_i + \overline{U_i}$$
$$p = P + \overline{P} \qquad (4.5)$$

Where $\overline{U_i}$ and $\overline{P}$ denote the time-averaged quantities while U_i and p are the fluctuating components of the velocities and the pressure. By inserting the Reynolds decomposition into the Navier-Stokes equations given in equation (4.1), the Reynolds averaged Navier-Stokes (RANS) equations are obtained. These are written as

$$\frac{\partial \overline{U_i}}{\partial x_i} = 0.0$$

$$\frac{\partial \overline{U_i}}{\partial t} + \overline{U_j}\frac{\partial \overline{U_i}}{\partial x_j} = -\frac{1}{\rho}\frac{\partial \overline{P}}{\partial x_i} + \nu\frac{\partial^2 \overline{U_i}}{\partial x_j \partial x_j} - \frac{\partial \overline{u_i u_j}}{\partial x_j} + g_i \qquad (4.6)$$

It can be noted that the RANS equations are very similar to the Navier-Stokes equations except for the additional term including $u_i u_j$, referred to as the Reynolds stress tensor. If the Reynolds stress term is modelled, the RANS equations describe the time-averaged flow quantities which require substantially less computational resources in comparison to DNS.

A common approach for modelling the Reynolds stress tensor of the RANS equations is to use the Boussinesq approximation. In this assumption, the Reynolds stress tensor is modelled as a diffusion term by introducing a turbulent viscosity, νt, according to

$$-\overline{u_i u_j} = \nu_t\left(\frac{\partial \overline{U_i}}{\partial x_j} + \frac{\partial U_j}{\partial x_i}\right) - \frac{2}{3}k\delta_{ij} \qquad (4.7)$$

In this equation, δ_{ij} is the Kronecker delta which assumes a value of 1 if i = j and 0 otherwise, and k is the turbulent kinetic energy defined as

$$k = \frac{1}{2}\overline{u_i u_j} \qquad (4.8)$$

By using a model to describe how the turbulent viscosity depends on the flow, the RANS equations can be solved. The so-called two-equation turbulence models, such as the k-ε model and the k-ω model, use two additional

transport equations to describe the turbulent viscosity. They are referred to as complete models since they allow the turbulent velocity and length scales to be described independently [30].

4.2.3 Turbulence Model Standard k-ε

The stander k-ε model reported by Launder et al., to obtain turbulent viscous using transport equation for turbulence kinetic energy k

$$\frac{\partial(\rho k)}{\partial t} + \frac{\partial(\rho k \overline{U}_i)}{\partial x_i} = \frac{\partial}{\partial x_j}\left(\left(\mu + \frac{\mu_t}{\sigma k}\right)\frac{\partial k}{\partial x_i}\right) + P_k - \varepsilon\rho \quad (4.9)$$

And transport equation for dissipation rate ε

$$\frac{\partial(\rho\varepsilon)}{\partial t} + \frac{\partial(\rho\varepsilon\overline{U}_i)}{\partial x_i} = \frac{\partial}{\partial x_j}\left(\left(\mu + \frac{\mu_t}{\sigma\varepsilon}\right)\frac{\partial\varepsilon}{\partial x_i}\right) + \frac{\varepsilon}{k}(C_{\varepsilon 1}P_k - C_{\varepsilon 2}\varepsilon\rho) \quad (4.10)$$

To obtain

$$\mu_t = C_\mu \frac{\rho k^2}{\varepsilon} \quad (4.11)$$

Where

σk, $\sigma\varepsilon$ and C_μ are model constants

$C_{\varepsilon 1}$ and $C_{\varepsilon 2}$ are variable coefficient for the model

P_k is the production due to mean velocity shear

Table 1 shows the model coefficients improved during the time by a group of scientists.

Table 1. model coefficients improve with time

model	years	C_1	C_2			
Launder and Jones	1972	1.55	2	1.3	1	0.9
Sharma and Launder	1974	1.44	1.92	1.3	1	0.9
Spalding and Launder	1974	1.44	1.92	1.3	1	0.9

The turbulence *k-ε* has a reasonably accurate and computational cost per iteration compare with most anther turbulence models, resulting in that it used the engineering turbulence model for industrial applications. There is constrain for turbulence model at a wall, strong separation, curvature and large streamline for that must be using the wall function.

4.2.4 Turbulence Model k-ω

The turbulence model *k-ω* reported by Wilcox [31]. It has a transportation equation for kinetic energy *k* and specified dissipation *ω*, this specific dissipation has a relation to dissipation *ε* according to

$$\omega \propto \frac{\varepsilon}{k} \quad (4.12)$$

$$\frac{\partial k}{\partial t} + \frac{\partial}{\partial x_i}(k\overline{U}_i) = \frac{\partial}{\partial x_j}\left(\left(\nu + \frac{\nu_t}{\sigma_k^\omega}\right)\frac{\partial k}{\partial x_j}\right) + P_k - \beta^* k\omega \quad (4.13)$$

And transport equation for

$$\frac{\partial\omega}{\partial t} + \frac{\partial}{\partial x_i}(\omega\overline{U}_i) = \frac{\partial}{\partial x_j}\left(\left(\nu + \frac{\nu_t}{\sigma_\omega}\right)\frac{\partial\omega}{\partial x_j}\right) + \frac{\omega}{k}(C_{\omega 1}P_k - C_{\omega 2}k\omega) \quad (4.14)$$

To obtain

$$\nu_t = \frac{k}{\omega} \quad (4.15)$$

Where

β^*, , σ_ω, $C_{\omega 1,}$ and $C_{\omega 2}$ are model constants.

The merits of this turbulence model have good work near the wall and low turbulent regions [29]. Hence, it is valid too in the regions of turbulent Reynolds number locale near to the wall, lead to that the transport equations can be utilized within the entire stream space. The disadvantage of the *k-ω* model is that the results are sensitive to the choice of boundary conditions and initial conditions.

4.2.5 Turbulent Model SST

Shear stress transport (SST) model described by Menter. This model is a hybrid turbulence model to get advantages *k-ε* and k-ω turbulent models. Figure 16 shows the Zonal work turbulence model *k-ε* & k-ω around the flat plate, the first model applies in the wake and outward stream domain. Other models work around the wall it means sub and log layer.
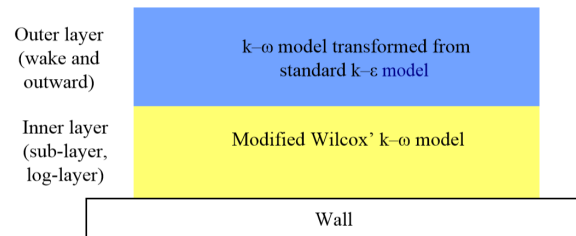
Figure 16. Zonal work turbulence model *k-ε* & *k-ω* on a flat plate [32]

According to a combination between k-ε and k-ω turbulence models, Transportation equation blended of them to obtain by

$$\frac{\partial(\rho k)}{\partial t} + \frac{\partial(\rho k\overline{U}_i)}{\partial x_i} = \frac{\partial}{\partial x_j}\left(\left(\mu + \frac{\mu_t}{\sigma k}\right)\frac{\partial k}{\partial x_j}\right) + \tau_{ij}\frac{\partial\overline{U}_i}{\partial x_j} - \beta^*\varepsilon\rho\omega$$

$$\frac{\partial\omega}{\partial t} + \frac{\partial}{\partial x_i}(\omega\overline{U}_i) = \frac{\gamma}{\nu_t}\tau_{ij}\frac{\partial\overline{U}_i}{\partial x_j} - \beta\rho\omega^2 + \frac{\partial}{\partial x_j}\left(\left(\mu + \frac{\mu_t}{\sigma_\omega}\right)\frac{\partial\omega}{\partial x_j}\right) + 2\rho(1 - F_1)\sigma_{\omega 2}\frac{\partial\omega}{\partial x_j}\frac{\partial k}{\partial x_j}\frac{1}{\omega} \quad (4.16)$$

The SST *k-ω* model has shown good performance for many types of complex flows, such as inflows with adverse pressure gradients and separating flows. It has been recognized for its good overall performance [33] and it is the most commonly used turbulence model for simulations of ship hydrodynamics. A drawback needs a lot of time to solve problems combers with the *k-ε* turbulence model.

4.3 Geometry of Planing Hull

The model employed in this study is the same as the one used in the Morabito experiment [34] whose model surface is shown in Figure 17. The model is a box shape whose dimensions are (length 914 mm, beam 183 mm, depth 102 mm) with groove (9 mm high × 6 mm deep)

around the model. It is located at 9 mm above the bottom.

a) Experimental model (Morabito, 2013)
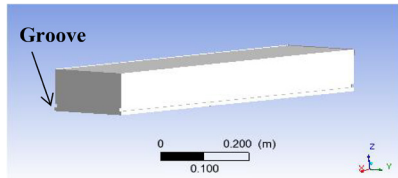
b) Numerical model

Figure 17. Planing hull model a) Experimental model (Morabito, 2013) b) Numerical model

The test was adopted by moving the model through the channel at a constant sinkage and trim by aft is equal to 6 degrees. This angle raises the bow of the hull above the waterline leads to canceling the bow effect. The hull model is examined in calm water at a range of speed from 0.3 m/s to 3.7 m/s for water depths 0.5b, 0.75b, 3b, 8b.

The objectives of the Morabito experiment are to measure the tangential force and normal force on the bottom of the hull separately using a dynamometer, also it's calculated; the change in wetted chain length (L_C), and transom ventilation (Y_K) at all range of speed. For that, the hull is divided into station and water line shown in a.

4.4 Planing Hull Computational Domain

Due to the symmetry of the hull, only half of the computational domain is represented in the CFD simulations of this study with dimensions shown in Figure 18. The hull is implemented with a fixed trim of 6 degrees and fixed heave giving a transom draft of 0.05673 m, such as that in the experimental work. The study is carried out to simulate a shallow channel whose water depth is 0.1 L and width is 1.3 L. The reference point of the computational domain is at G= (0, 0, 0). Boundary conditions imposed on the numerical domain are shown in Table 2. The air-water flows through the shallow channel from inlet to outlet about the hull. These investigations cover a range of speeds from 0.3 m/s to 3.7 m/s. This range includes the three regions of the subcritical, critical, and supercritical speeds. Also, when the analysis for deep water, the high seabed equal to 2.46 L. This height ensures no effect for seabed on the hull resistance.
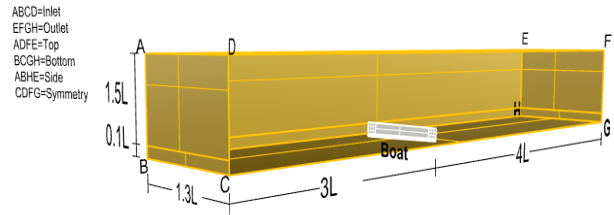
Figure 18. Dimension and boundary conditions of the shallow domain

Table 2. boundary conditions details

Position	type	boundary condition
Boat	No-slip	wall
Inlet	velocity	inlet
Outlet	static pressure	outlet
Top	free slip	wall
Side	free slip	wall
Bottom	free slip	wall
Symmetry	-	symmetry

In this investigation, was selected the *k-ε* turbulence model depending on previous work [12]. At the critical speeds, when the ship velocity is equal to the velocity of the wave in a shallow channel, the solitary wave will be established every some time. The solitary waveform is a wave single crest that moves forward through the shallow channel. Hence, it's required transient analysis at critical speed as shown in Table 3. The analysis at subcritical speeds and supercritical speeds are steady with time shown in Table 4.

Table 3. analysis setting at critical speeds

analysis type	transient
number of element	6000000
turbulent model	*k-ε*
Total time	25 sec
time step	0.2 sec

Table 4. analysis setting at subcritical and supercritical speeds

analysis type	Steady-state
number of element	6000000
Residual	e^-5
Max iteration	10000
turbulent model	*k-ε*

4.4.1 Open Water Domain Dimension

An open water analysis needs to make some changes

in computational domain dimensions to cancel the seabed effect shown in Figure 19. When $h/T \geq 10$ the effect of seabed to the hull is insignificant. In literature reviews of planing hull analysis in deep water, the depth of water is equal to three times the total length of the vessel. Moreover, the distance between the channel side and the hull equals two and a half time the hull length. This distance more than enough to remove the effect of channel-side into the hull. The small box around a hull as a domain uses to help capture physics phenomena at deep-water analysis. A small domain dimension is shown in Figure 19.
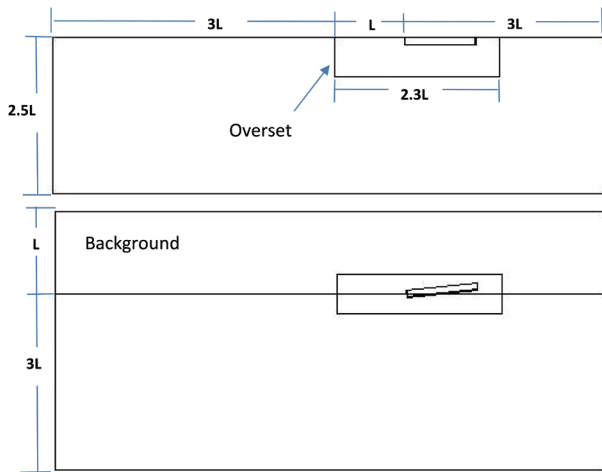
Figure 19. Open water domain dimension

4.4.2 Distribution on the Hull

In the current study, the wall bounding effects are very important and have a significant effect on the hull form drag at different speeds. Figure 20 shows the distribution y+ on the hull which a value around 30 to 300. This range of y+ gives the turbulence model a good chance to predict the flow around the hull form properly. Can be calculated.

$$y^+ = \frac{yu^*}{v} \qquad (4.17)$$

u^* Calculated by flowing formula

$$u^* = \sqrt{\frac{t_w}{\rho}} \qquad (4.18)$$

And

$$t_w = \frac{1}{2} \rho \, C_f U^2 \qquad (4.19)$$

The distance from the surface of the hull to the first cell centroid considered it y, u^* wall friction velocity, v kinematic viscosity, t_w sheer stress, ρ dynamic viscosity, U speed of the vessel, C_f friction coefficient obtained by equation (4.3).

4.4.3 Free Water Surface

To simulate a hull moving in water, models are needed to resolve the interface between the water and air. There

are different two-phase models available that either tracks the surface directly or tracks the different phases and then reconstruct the interface. One example is the level-set
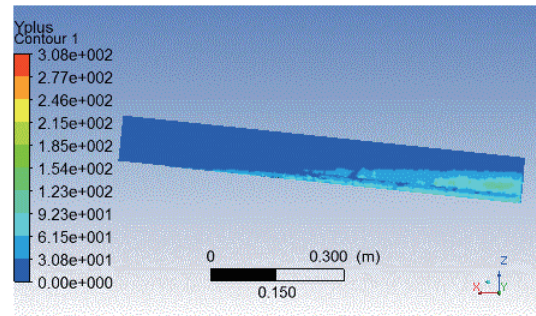
a) hull side in shallow water
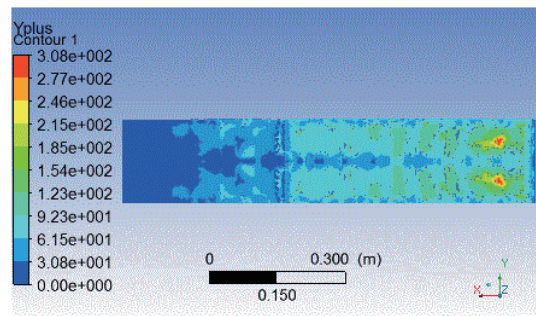
b) hull bottom in shallow water
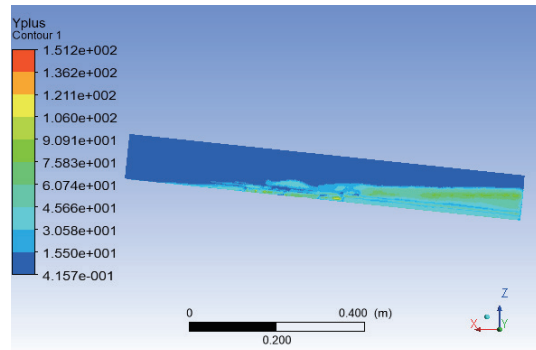
a) hull side in open water
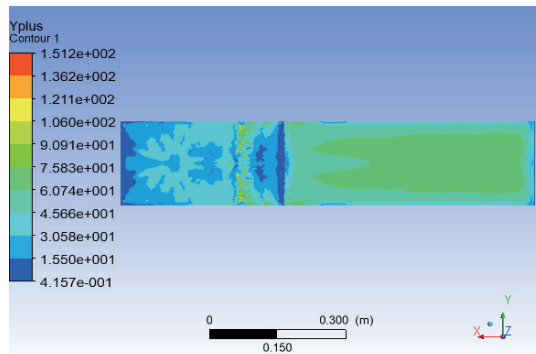
b) hull bottom in open water

Figure 20. distribution y+ on the hull

method, where all molecules of one phase are marked and then tracked in the fluid flow. The most frequently used

method to capture the free surface in ship hydrodynamics is the volume of fluid (VOF) method. In the VOF method, the different phases are tracked.

The flow of the model is assumed to be an incompressible turbulent flow. Hence, the governing equations are the continuity and momentum equations given as follows.

$$\frac{\partial u}{\partial x} + \frac{\partial v}{\partial y} + \frac{\partial w}{\partial z} = 0$$

$$\frac{\partial \overline{U_i}}{\partial t} + \overline{U_j}\frac{\partial \overline{U_i}}{\partial x_j} = -\frac{1}{\rho}\frac{\partial \overline{P}}{\partial x_i} + \nu\frac{\partial^2 \overline{U_i}}{\partial x_j \partial x_j} - \frac{\partial \overline{u_i u_j}}{\partial x_j} + g_i \quad (4.20)$$

The Reynolds stress tensor $\overline{u_i u_j}$ represents the change of momentum cross the free-surface which occurs as a result of surface tension force, the color function describes the free-surface as the volume of fraction γ

$$\frac{\partial \gamma}{\partial t} + U_i\frac{\partial \gamma}{\partial x_i} = 0 \quad (4.21)$$

Based on the volume of fluid (VOF) method, the air-water interface is described implicitly. The volume of fraction γ represents the percentage of water at each cell at the free surface to describe the interference between the two fluids. The magnitude of γ for each cell cut by the free surface is between 0 and 1 ($0 < \gamma < 1$). While the volume fraction γ equals 1 for total water occupancy, it equals 0 for total air

$$\rho_{ij} = \gamma_{ij}\rho_w + (1 - \gamma_{ij})\rho_a \quad (4.22)$$
$$\mu_{ij} = \gamma_{ij}\mu_w + (1 - \gamma_{ij})\mu_a \quad (4.23)$$

Where ρ and μ at any cell (denoted by ij) can be computed using γ by taking a simple volume average over the cell. Besides, (a) and (w) refer to air and water, respectively.

4.5 Mesh Generation Strategy

Code ICEM CFD is used to generate an unstructured mesh grid required for the CFD code solver.

For analysis in two waterways, it needs different strategies for building mesh in the computational domain. In shallow channel analysis is applied grid in one-domain is called single mesh, whereas a two-domain grid is used in open water analysis it is called overset mesh.

4.5.1 Single Mesh

The number of mesh elements generated –in one domain- and shown in Figure 21 equals 6 million elements. The accuracy of results is dependent on the quality of the mesh grid which is affected by the element size, type, and algorithm. The number of mesh elements is increased over the planing hull surface and its vicinity to improve the accuracy of numerical predictions of resistance and wave patterns generated at different forward speeds. The mesh density function is applied at the free-surface region throughout the whole computational domain to better predict the generated wave patterns by the hull. A refined mesh is generated at the bottom of the computational domain to accurately predict the effect of the channel bottom on the hull resistance.
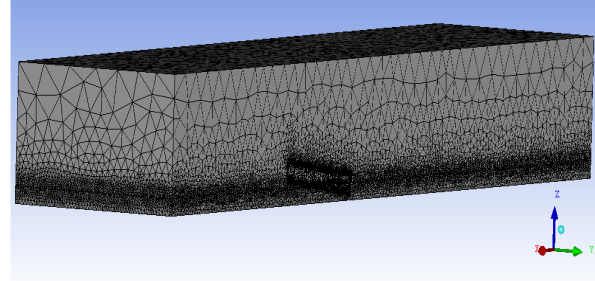
a) Tetrahedral mesh all over the domain
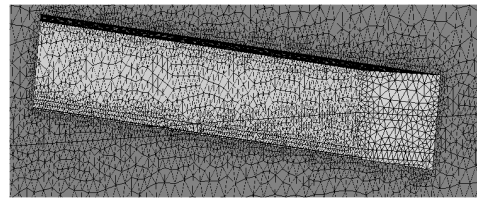
b) Mesh size around the hull

Figure 21. Schematic illustration of generated 6 million mesh elements in one-domain. A) Tetrahedral mesh all over the domain b) Mesh size around the hull.

4.5.2 Overset Mesh

The overset mesh creation is a bit more challenging than the one of the single mesh since it requires the creation of two computational domains: the background and the overlapping domain. The first one consists of a box of large dimensions, while the second one is smaller and contains the boat shown in Figure 19. The idea underlying the overset technique is that the increasing number of elements mesh around the hull without increase the total number of elements in the background domain. On the other hand, the drawback lays in the fact that there has to be communication between the two domains, through an interpolation across the domain boundaries of the smaller domain. To limit the effect of the interpolation to the minimum the meshes have to be built so that the size of the cells at the boundary of the overlapping domain is as close as possible to one of the background domains in that area. Once the domains are created, the same refinements presented for the single mesh are applied, with the only difference that some refinements will belong to the overset domain and some to the background. The free surface refinement will belong to both: an internal surface needs to be created in both domains. The wake refinement will be present only in the background domain,

while the surface, curve, and undersea refinements will be added in the overset one. Another refinement is added in the background domain, to comply with the requirement of the same cell size in the area around the boundaries of the overset domain. This is done by inserting in the background domain a box refinement around the overset domain with a target cell size of 0.04 m. Figure 22 shows tetrahedral mesh around the two domains and presium layer around the hull.
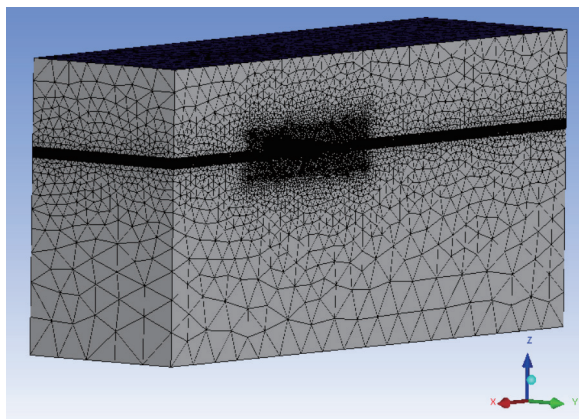
a) Tetrahedral mesh all over the domain
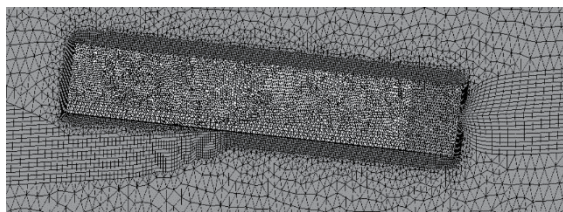
b) Presium layer around the hull

Figure 22. overset mesh generation 1.6 million mesh element

4.6 Mesh Dependence Study

The one-domain mesh generation gives a tremendous number of elements when the change element size. To improve the results a grid dependence study has been made for three generations of mesh 3, 6, and 9 million elements. The grid which has 6 million elements give the best results for all range of speeds and suitable time of analysis. Table 5 shows the error of numerical results for three mesh element comber with experimental resistance and lift force. The minimum error can be founded for the last speed in the range of critical speed 1.2 m/s achieved by 6 million elements.

4.7 Solution

When achieved convergence criteria for total resistance and lift force, the analysis was completed to solve the problem. Figure 30 explains the value of total resistance, lift force, and trim moment in the critical speeds range.

4.8 Post-processing

After the analysis was finished, the post-processing tool was utilized to describe the contour in the waterline, dynamic pressure contour on the hull, and the relation between time and resistance or force or trim moment.

5. Results and Discussion

This study predicted total resistance, generated wave pattern and, lift force of a planing hull model moving in a shallow channel over three regions of speed, (subcritical, critical, and supercritical). Numerical results were validated by comparison with experimental data available in the literature [14].

5.1 Comparison of Numerical and Experimental Results

This part of the thesis compares to available experimental results; wetted length, dynamic normal force over displacement, and lift force coefficient with the numerical results. Notice that, at the critical speed range the value of results fluctuates. For that, the mean value was obtained numerically and compared with the mean value experimentally. The mean value of results can be calculated as

$$Xm = \frac{\sum_{k=1}^{k=n} X_k}{n} \tag{5.1}$$

Where

X_m = mean result at a critical speed

n = number of results

X_k = results at a critical speed.

Furthermore, the percentage of error calculated from this equation:

$$error = \left|\frac{V_{ex} - V_{nu}}{V_{ex}}\right| * 100\% \tag{5.2}$$

Where

V_{ex} = experimental value

V_{nu} = numerical value

Table 5. mesh dependence study for speed 1.2 m/s

Force on hull (N)	Experimental (N)	3 Million Elements	Error (%)	6 Million Elements	Error (%)	9 Million Elements	Error (%)
Total Resistance	4.80	6.64	38	6.08	27	6.33	32
Lift Force	41.75	58.98	41	56.03	34	58.00	39

5.1.1 Comparison SST & k-ε Turbulence Model

The results of the total resistance are calculated from two turbulences mode SST & *k-ε*. The SST model spends more time to arrive at the result comber with the k-ε model. Because the SST model solves two transport equations. Table 6 shows comparison between two errors of total resistance when using SST & *k-ε* model. In the SST turbulence model, the error of resistance is near to 1% in middle high speeds. Whereas in last high speed the error of the k-ε model lower than an error of the SST model. After that, the error of an SST and k-ε model are Convergent in all ranges of speed. In this investigation was selected the *k-ε* turbulence model for all range of speeds.

Table 6. comparison total resistance using turbulent mode SST and k-ε

Velocity (m/s)	$R_{T,Exp}$ (N)	R_T (*k-ε*) (N)	R_T (SST) (N)	(*k-ε*) Error 100%	(*SST*) Error 100%
0.3	0.309	0.307	0.307	0.555	0.606
0.5	0.670	0.789	0.798	17.792	19.041
0.6	1.215	1.123	1.202	7.506	1.050
0.8	2.513	2.755	2.755	9.642	9.642
0.9	3.736	3.582	3.473	4.134	7.058
1	4.416	4.294	4.227	2.759	4.284
1.1	4.946	5.351	5.298	8.189	7.119
1.2	4.801	6.080	6.011	26.628	25.201
1.3	4.787	4.905	4.793	2.458	0.115
1.4	4.856	5.049	4.904	3.983	0.993
1.5	5.007	5.214	5.051	4.137	0.882
1.8	5.814	5.792	5.588	0.374	3.879
2.4	7.737	7.255	6.958	6.225	10.066
3	9.771	9.029	8.660	7.596	11.371
3.7	12.379	11.645	11.172	5.928	9.753

5.1.2 Wetted Length Lc

The wetted length expresses the chine length under the waterline

Figure 23 shows the comparison between the wetted length to beam ratio of the model versus Froude depth numerically and experimentally. When the Froude depth near 1, the wetted length increases, as a result of solitary wave formation at the critical speeds range. However, all the ranges of numerical results achieved an error of around 4.8 % compared with experimental results. The maximum error at F_h= 1.27 is equal to 31.3 %. Approximately, at the supercritical speeds range, the wetted length is steady at 3.45 while, at subcritical speeds, it's slightly fluctuated around 3.25. In general, the numerical results of Lc/b showed an excellent agreement with the results of the experiment.
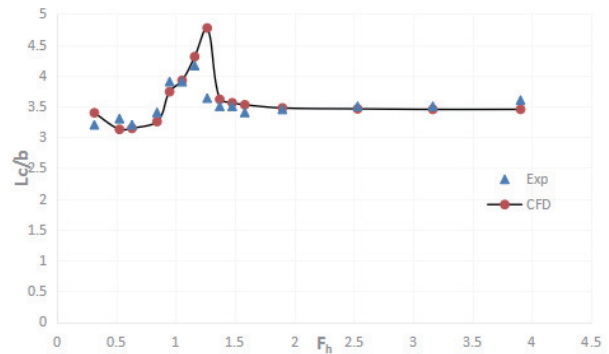
Figure 23. Comparison between experimental and CFD results of wetted length/beam ratio at different Froude depth

5.1.3 Normal Force (N)

The normal force means the hydrodynamic force acts perpendicularly to the hull bottom. Figure 24 shows the dynamic normal force to static buoyancy force ratio, versus the Froude beam (C_V) numerically and experimentally. The experimental normal force ratio slightly decreases below zero at the low-speed range before full ventilation at the transom occurs, which means the dynamic force applies suction on the hull toward the channel bed (squat force). The numerical normal force slightly decreases at partial ventilation. Then it increases rapidly until the dynamic force equal to displacement force at full ventilation at transom as a result of hydrodynamic lift. At this range the largest deviation between experimental and numerical results occurs. After that, the curve increases sharply without a considerable deviation between numerical and experimental results. The numerical results are lined with experimental results.
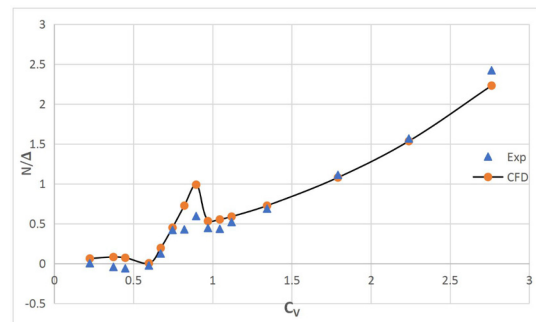
Figure 24. dynamic normal force/static normal force ratio N/Δ versus C_v numerically and experimentally

5.1.4 Total Resistance RT

A comparison between the numerical total resistance and experimental total resistance is shown in Figure 25. The two curves increase sharply over the critical Froude

number's range (Fh=0.84 to Fh=1.27). After that, there is a slight drop in values and then they increase gradually over the supercritical Froude number's range (Fh=1.37 to Fh=3.9). Very good agreement between the two curves is observed over –almost- the whole range of Froude numbers albeit, the error increases at Froude number close to the peak. The total average error between the numerical and experimental total resistance is no more than 8%. The maximum error is observed at the maximum critical Froude-depth number of 1.27 and is equal to 26%.
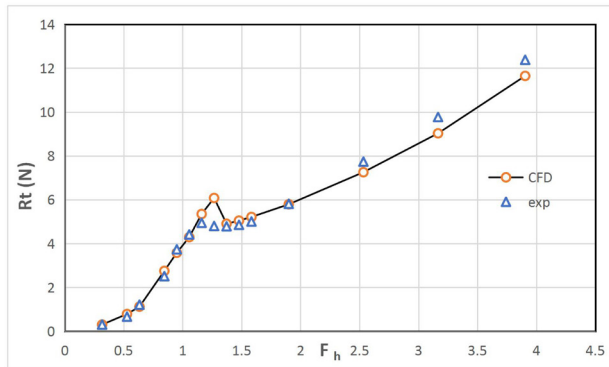
Figure 25. Experimental and numerical total resistance

5.1.5 Hydrodynamic Lift Force LF

A comparison between the numerical and experimental total lift force is shown in Figure 26. In general, the lift force decreases slightly over the supercritical range (from F_h=0.32 to F_h=0.63). There is a numerical over prediction of the lift force in this range. However, the lift force increases rapidly over the critical speed range (from F_h=0.84 to F_h=1.27). Subsequently, the value of the lift force rises gradually over the supercritical range. The total average error equals 7%, while the maximum error is 34% at the maximum critical Froude-depth number. For the whole range of speeds, very good agreement is observed between the numerical and experimental lift force except the maximum critical speed of 1.2 m/s.
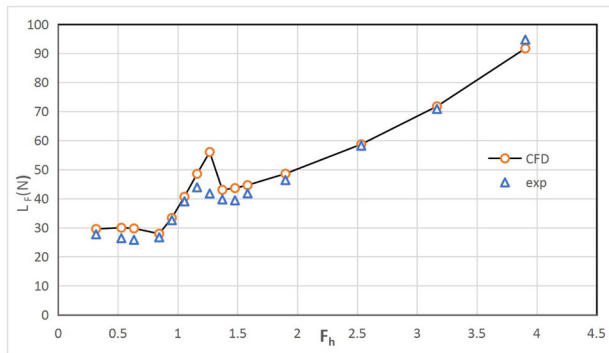
Figure 26. Experimental and numerical Lift force

5.1.6 Wave Pattern

The numerical and experimental wave pattern is similar at speed 0.3 m/s as shown in Figure 27. The free surface deformation at the displacement speed of 0.3m/s is not significant. In the low-speed region, there is no high deformation at the hull side, the wetted chine experimentally and numerically equal to 558.8 mm and 620.9 mm sequentially. Also, there is partial ventilation at transom equals 2.12 mm experimentally and 3.23 mm numerically.
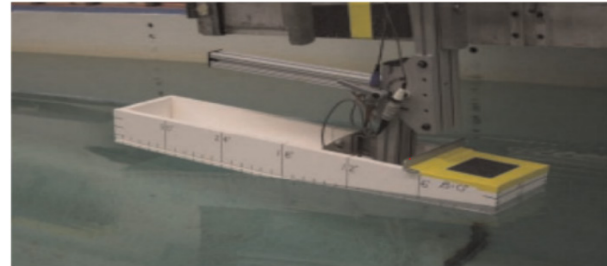
a) Experimental Wave pattern [34]
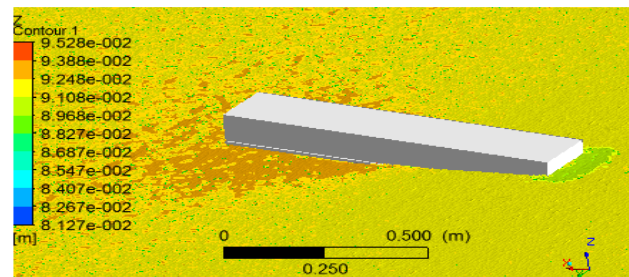
b) Numerical wave pattern

Figure 27. Wave pattern comparison at speed of 0.3 m/s

Figure 28 shows a similarity in the generated wave pattern numerically and experimentally at a speed of 1.8 m/s. There is a high deformation on the free surface at the planing speed of 1.8 m/s. While the waves about the hull side increase in height leading to an increase in wetted chine equal to 635.42 mm numerically and 609.6 mm experimentally, further the free surface drops at the transom. For the numerical and experimental generated wave pattern, high deformation occurs on the free surface and full ventilation at transom equal to 56.73 mm experimentally and 59.03 mm numerically.
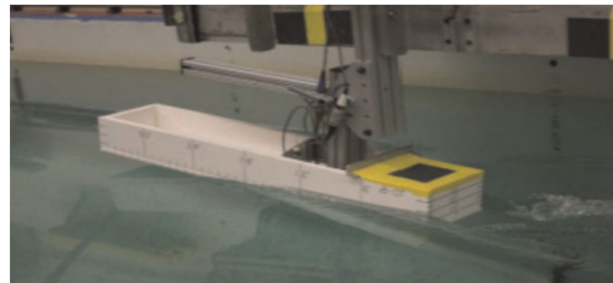
a) Experimental wave pattern [34]
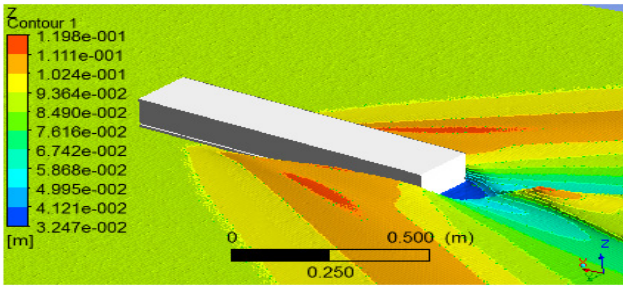
b) Numerical wave pattern

Figure 28. Wave pattern comparison at speed 1.8 m/s

5.2 Solitary Wave Formation and Effects

In this section, the complex hydrodynamic phenomena of solitary wave or soliton formation will be discussed. The solitary wave requires a specific situation to occur such as a shallow channel waterway. When a hull is moving at critical speed in a shallow channel, the solitary wave will be observed. Table 7 shows the solitary waves establishment positions, and amplitudes for critical speeds which are 0.8, 0.9, 1, 1.1, 1.2 m/s. The amplitude of the solitary wave increases with the increase in wave speed. At speed 1.2 m/s, the generated solitary wave is at amidships which has the highest amplitude of 0.05960 m. The solitary wave shifts forward till positioned at the front of the hull, which leads to fluid flow about the hull to be more complex.

Table 7. properties the solitary wave at a range of critical speed

Critical speed m/s	location of the wave formation numerically	Maximum wave amplitude (m)	location of the wave formation experimentally
0.60	No wave	-	No wave
0.80	3.3m ahead of model	0.0133	3 m ahead of model
0.90	1.2m ahead of model	0.0263	1 m ahead of model
1.00	0.3m ahead of model	0.035	at Bow
1.10	at Bow	0.0414	at Amidships
1.20	at Amidships	0.0596	supercritical swept 10-deg

The solitary wave establishes itself at different locations along the hull within the range of critical speeds and moves forward on the hull with time. Figure 29 shows the solitary wave formation steps. Firstly, the divergent waves hit the channel side at t = 2.4 seconds and increase the pressure on the channel sidewall. Secondly, the waves are reflected from the channel side and encounter other divergent waves generated from the hull after 4 seconds. Thirdly, the solitary wave becomes Perpendicular to the hull at t = 10 seconds. Afterward, the wave shifts forward at t = 14.2 seconds until the maximum amplitude

formulates at a position of 0.3m after the hull. The next pulse of the wave is produced at t = 18 seconds. As the hull moves in a shallow channel, it produces a pulse wave repeated every 23 seconds.
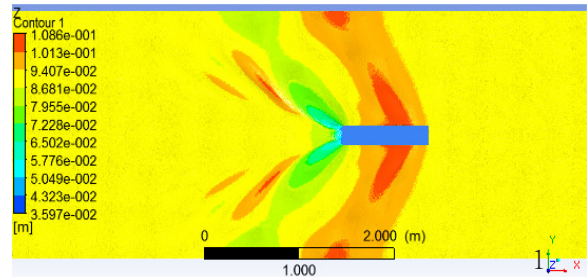
t=2.4sec
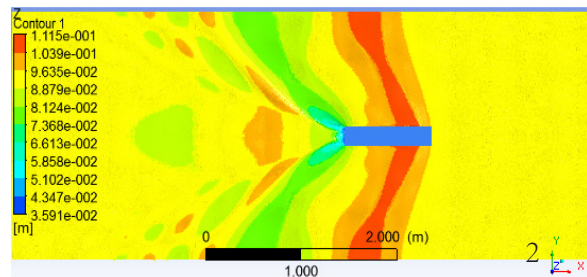
t=4sec
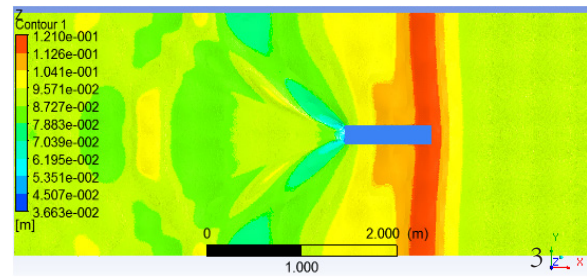
t=10sec
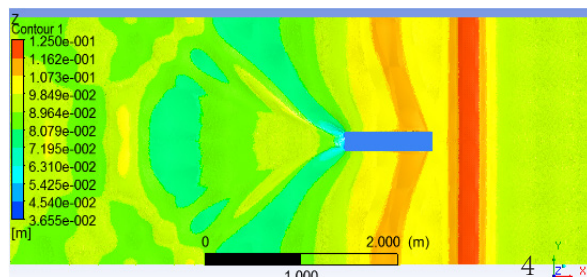
t=14.2sec
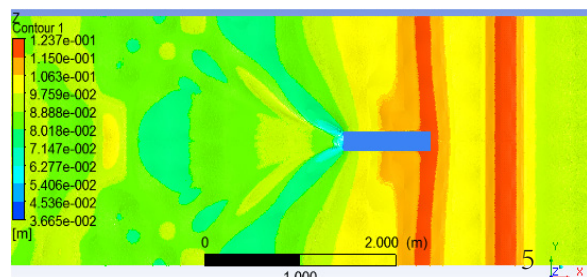
t=18sec

t=23sec
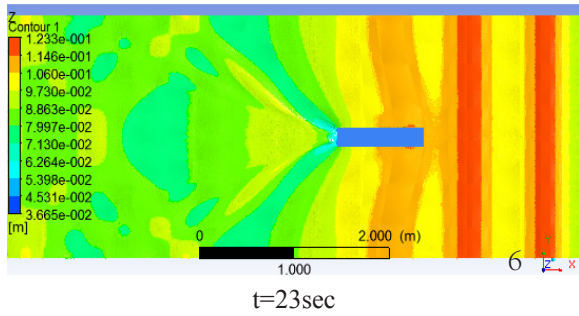
Figure 29. Solitary wave formulation steps at speed 1m/s

Figure 30 represents the change in a trim moment, lift force, and total resistance on a half planing hull at the critical speed versus time. The maximum trim moment and maximum lift force occur on the hull at the same time. The effect of a solitary wave on the moment and lift force curves is like a sinusoidal wave. The instantaneous values of the trim moment and lift force relate to the location of the solitary waveform and speed. The direction of a total resistance an opposite to inlet flow.

speed 1 m / s

Speed 0.8 m/s

Speed 1.1m/s
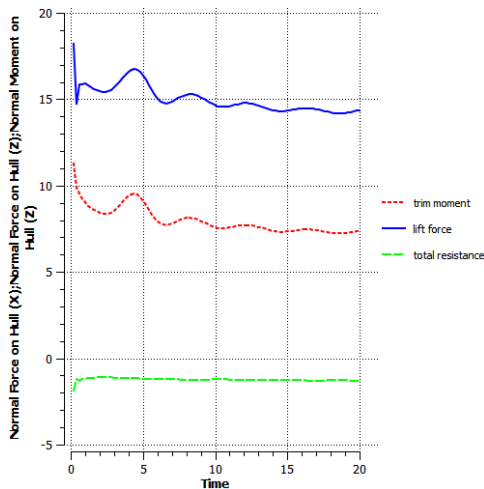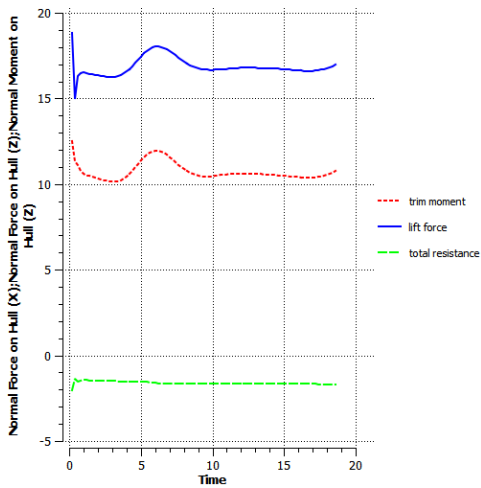
Speed 0.9 m/s

Speed 1.2 m/s
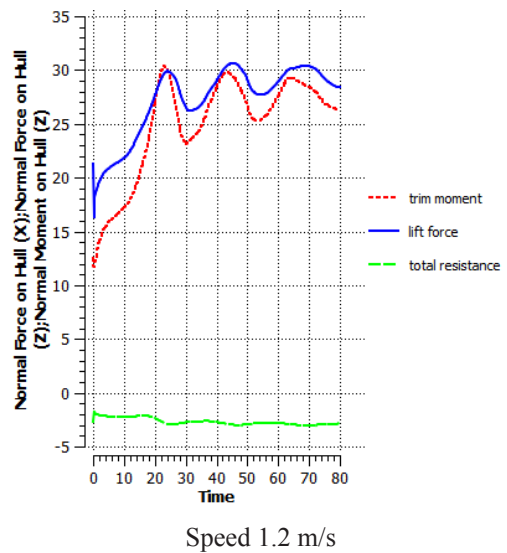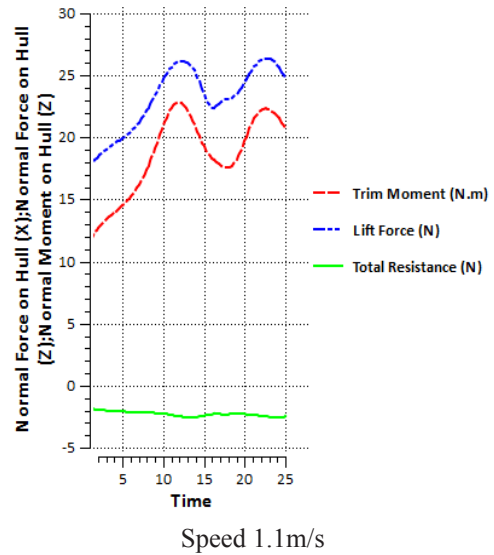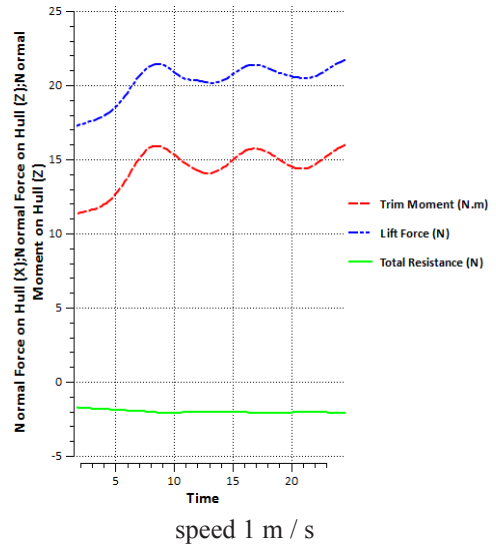
Figure 30. Solitary wave effects on a trim moment, lift force, and total resistance

5.3 Comparison between Hydrodynamic Performance in Shallow Water Channel and Open Water

In this section of a results comber, the dynamic pressures distribution on the hull, wave patter at critical speed, and total resistance change between shallow water channel and open water.

5.3.1 Dynamic Pressure Distribution on the Hull

Figure 31 shows the difference between the shallow channel and deep water hydrodynamic pressure around the hull at a critical speed.

Figure 31 (b) and (d) show an increased wetted surface area on the hull side and hull bottom in a shallow channel at critical speed compared with the wetted surface area in open water that is shown in Figure 31 (a) and (c). The maximum hydrodynamic pressure in Figure 31 (b) and (d) at hull piercing on the water. It's higher than that on the hull in (a) and (c). The pressure distributions around the hull at critical speed are unstable with time as a result of solitary wave formation.

5.3.2 Wave Pattern at Critical Speed

Figure 32 (a) and (b) show the wave elevation comparison between open water and shallow water channel at speed (1 m/s). The maximum wave height at the shallow water channel equals 0.069 m. On the other hand, the maximum wave height at deep water equals 0.038 m. The elevation of the wave in the shallow channel increases by about 81% from deep water. In shallow channels (Figure 32 (b)), the wave elevation increases, and the solitary wave occurs at a critical speed surface which leads to an increase in the wave-making resistance compared with open water.

5.3.3 Total Resistance (RT)

Figure 33 explains the total resistance in deep water for three regions of speed. When the Froude number is in the range of 0.5 this called displacement mode, and the total resistance increases with speed. For semi-displacement speed, the hump of resistance occurs at $0.5 < Fr < 0.85$ as a result of superposition in the wave system. After that, the total resistance increases with speed at the planing range $Fr > 0.85$. This general figure for the total resistance of the planing hull in deep water is similar to the deep water carve in Figure 34, which shows the total resistance in shallow water channels compared with the total resistance in deep water. The total resistance in deep water at low speeds is not exactly similar to the total resistance in the shallow channel. Firstly, in the deep water, the chart increases gradually until the appearance of the hump which increases resistance as a result of a superposition between two crests or two troughs in the wave system.

a) Pressure on hull side at deep water

(b) Pressure on hull side at shallow water

(C) Pressure on hull Bottom at deep water

(d) Pressure on hull Bottom at shallow water
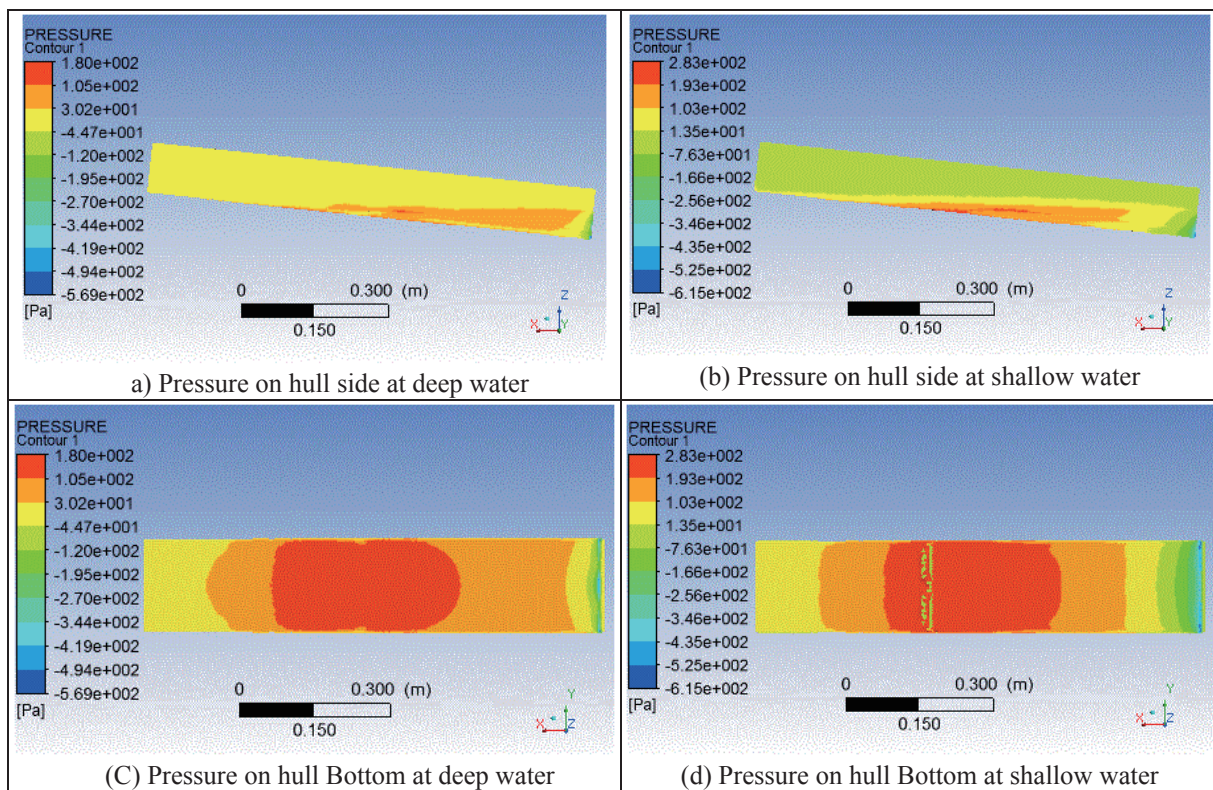
Figure 31. Hydrodynamic pressure around the hull

| (a) Wave elevation in a deep water | (b) Wave elevation in a shallow water |
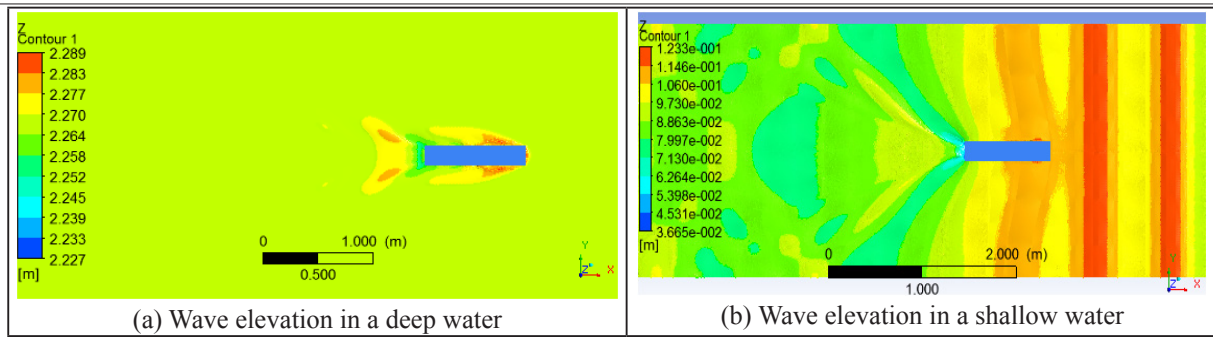
Figure 32. wave systems comparison between a shallow channel and open water at speed 1m/s

Also, there is a hollow that causes the total resistance to decrease because the crest cancels the trough in the wave system. Secondly, the total resistance in shallow water is rising rapidly in the critical speed period (0.8---1.2 m/s). The maximum difference between total resistance in shallow water and total resistance in deep water is equal to 43% at speed 0.9 m/s. The total resistance in the supercritical speed range increases dramatically with speed increase. Lastly, the total resistance in the shallow channel is much higher than the total resistance in open water.
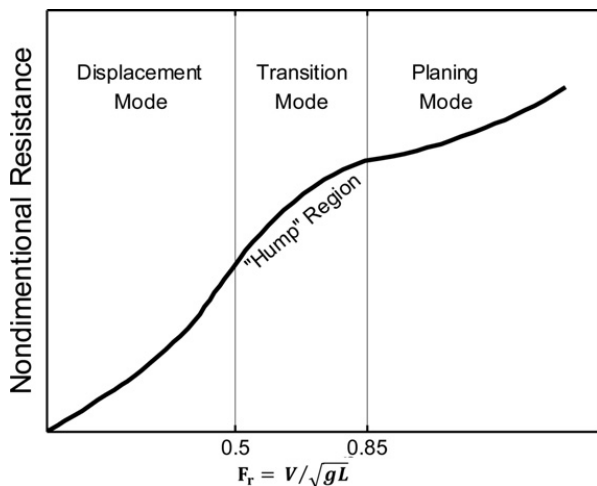
Figure 33. Total resistance of planing hull in deep water [35]
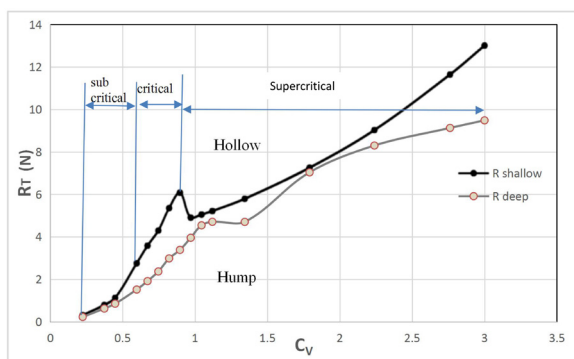
Figure 34. Comparison between the total resistance in shallow water channel and the total resistance in deep water

6. Conclusions and Recommendations

In this chapter, the conclusion, and recommendation of the results from the numerical simulations of the prismatic planning hull when moving in various waterways, is presented.

6.1 Conclusions

In this thesis, the RANS equations are solved by ANSYS-CFX code to simulate a small high-speed hull form moving in a shallow channel and open water. The total resistance and wave pattern of the planing hull model at three regions of speed (subcritical, critical, and supercritical) moving in the shallow channel have been numerically simulated.

• In the shallow water channel, the total average error equals 7% for numerical lift force, 8% for numerical total resistance compared with available experimental results. The numerical analysis well captured the wave pattern. The numerical results give good agreement over the whole range of speeds with the experimental results except at the maximum critical speed of 1.2 m/s which resulted in an error equal to 34% for lift force and 26% for total resistance.

• In the current study, the steps of the solitary wave formulation have been described at critical speeds. The amplitudes of the solitary waves were determined at the critical speeds of 0.8, 0.9, 1, 1.1, and 1.2 m/s where the amplitudes were found equal to 0.0133, 0.0263, 0.035, 0.0414, and 0.0596 m respectively.

• The amplitude of the solitary wave increases whenever there is an increase in the critical speeds. Also, this investigation defined the locations of the solitary wave formulation. Solitary wave formulates in front of the hull at the lower range of critical speed. However, at the higher range of critical speed, it formulates on the hull.

• The solitary wave formation increases the wetted surface area and the free surface deformation. Also, causes fluctuation in the trim moment, and lift force on the planing hull depends on the location and amplitude of the solitary wave. The total resistance on the hull in the

shallow channel is higher than the total resistance in open water. The maximum difference is 43% which takes place at a critical speed of 0.9 m/s.

In conclusion, the worst effect on the planing hull in shallow channels occurs at the critical speed range, where solitary wave formulates. So boat drivers must avoid sailing at a critical speed range.

6.2 Recommendations

The future working which can be recommended:

• Further study for critical speed ranges and behavior of hull motion especially the last speed in the range.

• Using various mesh strategies and different software for this investigation to do more verification of results.

• Additional research concerns the effect of channel dimensions and vessel shape on the formation of a solitary wave at a critical speed.

• Research on how to apply solitary wave energy in useful engineering applications.

References

[1] G. For et al., "GUIDELINES FOR WING-IN-GROUND CRAFT," Int. Marit. Orgnization, vol. 44, 2018.

[2] R. Yousefi, R. Shafaghat, and M. Shakeri, "Hydrodynamic analysis techniques for high-speed planing hulls," Appl. Ocean Res., vol. 42, pp. 105–113, Aug. 2013.
DOI: 10.1016/j.apor.2013.05.004.

[3] V. Kerman, "The Impact on Seaplane Floats During Landing," Washington, No 321, 1929.

[4] T. B.R, Savander, S.M, Scorpio, R.K, "Steady Hydrodynamic Analysis of Planing Surfaces," J. Sh. Res., vol. 46, pp. 248–279, 2002.

[5] S. D. S. Xue-Nong Chen, "A Slender Ship Moving at a Near-Critical Speed in a Shallow Channel," J. Fluid Mech., vol. 291, no. May 1995, pp. 263–285, 1995.
DOI: 10.1017/S0022112095002692.

[6] K. W. Christopher, "Effect of Shallow Water on the Hydrodynamic Characteristics of a Flat-Bottom Planing Surface." NACA, Washington, 1956, [Online]. Available: http://www.dtic.mil/cgi-bin/GetTRDoc?Location=U2&doc=GetTRDoc.pdf&AD=ADA377307.

[7] C. J. Reyling, "An experimental study of planing surfaces operating in shallow water," new jersey, 1976.

[8] A. Iafrati and R. Broglia, "Comparison between 2D+t potential flow models and 3d rans for planing hull hydrodynamics," Ital. Sh. Model Basin, no. December 2016, pp. 6–9, 1955.

[9] F. Di Caterino, R. Niazmand Bilandi, S. Mancini, A. Dashtimanesh, and M. DE CARLINI, "A numerical way for a stepped planing hull design and optimization," NAV Int. Conf. Sh. Shipp. Res., no. 221499, pp. 220–229, 2018.
DOI: 10.3233/978-1-61499-870-9-220.

[10] R. N. Bilandi, S. Mancini, L. Vitiello, S. Miranda, and M. De Carlini, "A validation of symmetric 2D + T model based on single-stepped planing hull towing tank tests," J. Mar. Sci. Eng., vol. 6, no. 4, 2018.
DOI: 10.3390/jmse6040136.

[11] S. Brizzolara and F. Serra, "Accuracy of CFD codes in the prediction of planing surfaces hydrodyamic characteristics," 2nd Int. Conf. Mar. Res. Transp., pp. 147–158, 2007, [Online]. Available: http://www.icmrt07.unina.it/Proceedings/Papers/B/14.pdf.

[12] A. S. Amir H. Nikseresht, "Numerical investigation of shallow water resistance of a planing vessel," Int. J. Civ. Struct. Eng., vol. 3, no. 1, pp. 164–168, 2016.
DOI: 10.15224/978-1-63248-083-5-62.

[13] S. Mancini, F. De Luca, and A. Ramolini, "Towards CFD guidelines for planing hull simulations based on the Naples Systematic Series," 7th Int. Conf. Comput. Methods Mar. Eng. Mar. 2017, vol. 2017-May, no. May, pp. 0–15, 2017.

[14] Y. Wang, "Numerical Prediction of Resistance of Planning Vessel with RANS Method," Int. Conf. Comput. Sci. Autom. Eng., no. Iccsae 2015, pp. 287–293, 2016.
DOI: 10.2991/iccsae-15.2016.55.

[15] A. De Marco, S. Mancini, S. Miranda, R. Scognamiglio, and L. Vitiello, "Experimental and numerical hydrodynamic analysis of a stepped planing hull," Appl. Ocean Res., vol. 64, pp. 135–154, 2017.
DOI: 10.1016/j.apor.2017.02.004.

[16] M. Bakhtiari, S. Veysi, and H. Ghassemi, "Numerical Modeling of the Stepped Planing Hull in Calm Water," Int. J. Eng., vol. 29, no. 2, 2016.
DOI: 10.5829/idosi.ije.2016.29.02b.13.

[17] A. Dashtimanesh, A. Esfandiari, and S. Mancini, "Performance prediction of two-stepped planing hulls using morphing mesh approach," J. Sh. Prod. Des., vol. 34, no. 3, pp. 236–248, 2018.
DOI: 10.5957/JSPD.160046.

[18] F. Roshan, A. Dashtimanesh, and R. N. Bilandi, "Hydrodynamic charactrisrics of tunneled planing hull in calm water," Brodogradnja, vol. 71, no. 1, pp. 19–38, 2020.

[19] A. Tafuni, I. Sahin, and M. Hyman, "Numerical investigation of wave elevation and bottom pressure generated by a planing hull in finite-depth water," Appl. Ocean Res., vol. 58, pp. 281–291, 2016.
DOI: 10.1016/j.apor.2016.04.002.

[20] D. Savitsky, "Hydrodynamic Design of Planing Hulls," Mar. Technol., vol. Vol. 1, no. No. 1, p. PP. 71-95, 1964.

[21] K. Potgieter, "Planing Hulls." South Africa, pp. 1–5,

2018.

[22] G. Fridsma, "A Systematic Study of the Rough-Water Performance of Planing Boats," 1969. [Online]. Available: http://oai.dtic.mil/oai/oai?verb=getRecord &metadataPrefix=html&identifier=AD0708694.

[23] F. De Luca and C. Pensa, "The Naples warped hard chine hulls systematic series," Ocean Eng., vol. 139, no. March, pp. 205–236, 2017. DOI: 10.1016/j.oceaneng.2017.04.038.

[24] F. M. White, Fluid mechanics, 7th ed. Boston: (Mcgraw-Hill series, 2003.

[25] M. Rabaud and F. Moisy, "Ship wakes: Kelvin or mach angle?," Phys. Rev. Lett., vol. 110, no. 21, 2013. DOI: 10.1103/PhysRevLett.110.214503.

[26] J. N. Newman, Marine Hydrodynamics, 40th ed. Cambridge: MIT press, 1977.

[27] D. Frisk and L. Tegehall, "Prediction of High-Speed Planing Hull Resistance and Running Attitude. A Numerical Study Using Computational Fluid Dynamics," CHALMERS UNIVERSITY OF TECHNOLOGY, Gothenburg, Sweden, 2015.

[28] W. M. H K Versteeg, An introduction to computational fluid mechanics., 2nd ed., vol. M. Pearson Prentic Hall, 2007.

[29] B. Andersson, R. Andersson, L. Håkansson, M. Mortensen, R. Sudiyo, and B. van Wachem, Computational Fluid Dynamics for Engineers. Cambridge University Press, 2011.

[30] L. Davidson, An Introduction to Turbulence Models. Gothenburg: Chalmers university of technology, 2018.

[31] D. C. Wilcox, Turbulence Modeling for CFD, Third edit. La Canada, California: DCW Industries, Inc, 2006.

[32] I. F. Training, "Modeling Turbulent Flows [REVISIT]," 2006, [Online]. Available: http://www.southampton. ac.uk/~nwb/lectures/GoodPracticeCFD/Articles/ Turbulence_Notes_Fluent-v6.3.06.pdf.

[33] T. Bardina, J., Huang, P., Coakley, "Turbulence Modeling Validation , Testing , and Development," California, 1997.

[34] M. G. Morabito, "Planing in Shallow Water at Critical Speed," J. Sh. Res., vol. 57, no. 2, pp. 98–111, 2013, doi: 10.5957/josr.57.2.120031.

[35] Marshall R, "All about Powerboats: Understanding design and performance," McGraw-Hill Professional, 2002.

Nomenclature
Latin Symbols

L	Length of planing hull (m)
B	Beam (m)
h	Depth of water (m)
U	Speed of the vessel (m/s).
g	Gravitational acceleration (m/s^2)
R_T	Total resistance (N)
R_V	Viscous resistance (N)
R_A	Air resistance (N)
R_S	Spray rail resistance (N)
R_M	Wave making resistance (N)
L_F	Lift force (N)
F_n	Froude number $F_n = U/\sqrt{g*L}$
Cv	Beam Froude number, $Cv = U/\sqrt{g*b}$
F_h	Depth Froude number $F_h = U/\sqrt{g*h}$
P	Pressure (N/m^2)
t_w	Sheer stress (N/m^2)
C_f	Frictional resistance
V	Speed of a wave (m/s)
Lc	Chine wetted length (m)
L_K	Length of the keel (m)
N	Dynamic normal force (N)
$C_{L\beta}$	Lift coefficient
C_{L0}	Lift coefficients at $\beta = 0°$
$F_{L\beta}$	Lift force (N)
F_{L0}	Lift force at $\beta = 0°$

Greek Symbols

α	Kliven angle (degree)
β	Deadrise angle (degree)
ρ	The density of the fluid (kg/m^3)
τ	Trim angle of planing hull (radian).
v	Kinematic viscosity (m^2/s)
λw	Mean wetted length-to-beam ratio, λw = $0.5(L_C + L_K/B)$, Taken rang λ$w \le 4$.
τ_{deg}	The trim angle of the planing hull (degree) take rang $2° \le \tau_{deg} \le 15°$

Abbreviation

FDM	Finite Different Method
FVM	Finite Volume Method
FEM	Finite Element Method
BEM	Boundary Element Method
2D	Tow dimension
3D	Three dimensions
VOF	Volume of Fluid
CFD	Computational Fluid Dynamic
RANSE	Reynolds Navier Stokes Equation
ACV	Air Cushion Vehicles
SES	Surface-Effect Ships
SWATH	Small water-plane-area twin-hull
ITTC	International Towing Tank Conference
PDE	Partial Differential Equation
DNS	Direct Numerical Simulation
SPH	Smoothed Particle Hydrodynamics

http://dx.doi.org/10.36956/sms.v3i1.414   55